

# Alternative angular variables for suppression of QCD multijet events in new physics searches with missing transverse momentum at the LHC

Tai Sakuma,<sup>a</sup> Henning Flaecher,<sup>a</sup> and Dominic Smith<sup>a,b</sup>

<sup>a</sup> *University of Bristol, Bristol, UK*

<sup>b</sup> *Vrije Universiteit Brussel, Brussel, Belgium*

*E-mail:* [tai.sakuma@bristol.ac.uk](mailto:tai.sakuma@bristol.ac.uk)

**ABSTRACT:** We introduce three alternative angular variables—denoted by  $\tilde{\omega}_{\min}$ ,  $\hat{\omega}_{\min}$ , and  $\chi_{\min}$ —for QCD multijet event suppression in supersymmetry searches in events with large missing transverse momentum in proton-proton collisions at the LHC at CERN. In searches in all-hadronic final states in the CMS and ATLAS experiments, the angle  $\Delta\varphi_i$ , the azimuthal angle between a jet and the missing transverse momentum, is widely used to reduce QCD multijet background events with large missing transverse momentum, which is primarily caused by a jet momentum mismeasurement or neutrinos in hadron decays—the missing transverse momentum is aligned with a jet. A related angular variable—denoted by  $\Delta\varphi_{\min}^*$ , the minimum of the azimuthal angles between a jet and the transverse momentum imbalance of the *other* jets in the event—is used instead in a series of searches in all-hadronic final states in CMS to suppress QCD multijet background events to a negligible level. In this paper, before introducing the alternative variables, we review the variable  $\Delta\varphi_{\min}^*$  in detail and identify room for improvement, in particular, to maintain good acceptances for signal models with high jet multiplicity final states. Furthermore, we demonstrate with simulated event samples that  $\hat{\omega}_{\min}$  and  $\chi_{\min}$  considerably outperform  $\Delta\varphi_{\min}^*$  and  $\Delta\varphi_i$  in rejecting QCD multijet background events and that  $\hat{\omega}_{\min}$  and  $\tilde{\omega}_{\min}$  are also useful for reducing the total standard model background events.

---

## Contents

<b>1</b>	<b>Introduction</b>	<b>2</b>
<b>2</b>	<b>Review of angle <math>\Delta\varphi_i^*</math></b>	<b>3</b>
2.1	Definitions	3
2.2	Geometric relations	4
2.3	Analytic properties	5
<b>3</b>	<b>Minimizing <math>H_T^{\text{miss}}</math> by varying jet <math>p_T</math></b>	<b>6</b>
3.1	Minimized $\vec{H}_T^{\text{miss}}$ and minimizing jet $\vec{p}_{T_i}$	7
3.2	Scale factor $\sin \Delta\tilde{\varphi}_i$ and ratio $g_i$	8
3.3	Relation to angle $\Delta\varphi_i^*$	9
<b>4</b>	<b>Simulated event samples</b>	<b>10</b>
<b>5</b>	<b>Minimized <math>H_T^{\text{miss}}</math> in QCD multijet events</b>	<b>12</b>
<b>6</b>	<b>Features of <math>\Delta\varphi_{\text{min}}^*</math> criterion</b>	<b>14</b>
6.1	Large $f_i$ and $f_{\text{max}}$	14
6.2	Wide $\Delta\varphi_i$ and jet $p_T$ overestimate	15
6.3	Narrow $\Delta\varphi_i$ —room for improvement	16
<b>7</b>	<b>Alternative angular variables: <math>\tilde{\omega}_{\text{min}}</math>, <math>\hat{\omega}_{\text{min}}</math>, <math>\chi_{\text{min}}</math></b>	<b>16</b>
7.1	Angle $\omega_i$	16
7.2	Variants of $\omega_i$	18
7.2.1	Angle $\tilde{\omega}_i$	18
7.2.2	Angle $\hat{\omega}_i$	19
7.2.3	Angle $\chi_i$	19
7.3	Alternative angular variables: $\tilde{\omega}_{\text{min}}$ , $\hat{\omega}_{\text{min}}$ , $\chi_{\text{min}}$	20
<b>8</b>	<b>Performance in simulated events</b>	<b>21</b>
<b>9</b>	<b>Summary</b>	<b>23</b>
<b>A</b>	<b>Event selection with <math>\widetilde{H}_{T\text{min}}^{\text{miss}}</math> and <math>X_{\text{min}}</math></b>	<b>26</b>
<b>B</b>	<b>Performance in Delphes samples with ATLAS card</b>	<b>27</b>
<b>C</b>	<b>Jet <math>p_T</math> resolution</b>	<b>27</b>
<b>D</b>	<b>Alternative angular variable <math>\xi</math></b>	<b>28</b>

---

# 1 Introduction

Supersymmetry (SUSY) searches in proton-proton collisions are ongoing at the CMS and ATLAS experiments at the LHC; recent results of searches in all-hadronic final states can be found, for example, in Refs. [1–14]. In SUSY models with  $R$ -parity conservation, SUSY particles are produced in pairs; then, their cascade decay chains each end with the lightest supersymmetric particle (LSP), which is typically the neutralino, *invisible* to the detectors, resulting in missing transverse momentum (denoted by  $\vec{E}_T^{\text{miss}}$  and its magnitude by  $E_T^{\text{miss}}$ ). For this reason, SUSY particles are usually searched for in events with large  $E_T^{\text{miss}}$ . In all-hadronic final states,  $\vec{E}_T^{\text{miss}}$  can be approximated by the missing transverse hadronic momentum (denoted by  $\vec{H}_T^{\text{miss}}$  and its magnitude by  $H_T^{\text{miss}}$ ), the negative vector sum of the transverse momenta ( $\vec{p}_T$ ) of all reconstructed *jets* in the event. Instead of or in addition to  $\vec{E}_T^{\text{miss}}$ ,  $\vec{H}_T^{\text{miss}}$  is often used in CMS [1, 2, 14].

In searches in all-hadronic final states, the angle  $\Delta\varphi_i$ —the azimuthal angle between a jet  $i$  and either  $\vec{E}_T^{\text{miss}}$  or  $\vec{H}_T^{\text{miss}}$ —is widely used to reduce QCD multijet background events with large  $E_T^{\text{miss}}$ , which is primarily caused by a jet mismeasurement or by neutrinos in hadron decays in a jet [1–4, 6–13]. The angle  $\Delta\varphi_i$  is narrow for the jet whose  $p_T$  is *underestimated* because of either a mismeasurement or neutrinos in hadron decays. In searches using  $\Delta\varphi_i$ , it is common to require the angles  $\Delta\varphi_i$  of only a few highest  $p_T$  jets in the event to be wider than thresholds, and the thresholds are sometimes narrower for jets with lower  $p_T$  rankings in the event [1, 3, 8, 9, 12, 13]. For example, the search in Ref. [1] required  $\Delta\varphi_i > 0.5$  for the two highest  $p_T$  jets and  $\Delta\varphi_i > 0.3$  for the 3rd and 4th highest  $p_T$  jets and had no requirement for the other jets.

It is uncommon to apply a lower threshold on the minimum of the angles  $\Delta\varphi_i$  of all jets in the event, in other words, to require all jets in the event to have  $\Delta\varphi_i$  wider than a certain angle, especially in high jet multiplicity events. This is because such a requirement would reduce too much the signal acceptances of SUSY models. In particular, signal events with high jet multiplicity have high chances to have at least one jet with narrow  $\Delta\varphi_i$ . Consequently, in common practice, a QCD multijet event with large  $E_T^{\text{miss}}$  caused by a jet  $p_T$  underestimate will not be rejected unless the jet whose  $p_T$  is underestimated is among the highest  $p_T$  jets in the event.

On the other hand, if the large  $E_T^{\text{miss}}$  in a QCD multijet event is due to a jet  $p_T$  *overestimate*, the angle  $\Delta\varphi_i$  of the jet whose  $p_T$  is overestimated is wide (near  $\pi$ ). However, it is also uncommon to apply an upper threshold on  $\Delta\varphi_i$  because this would also reduce signal acceptances too much. For example, jets in signal events that receive the recoil momenta of the LSPs have often wide  $\Delta\varphi_i$ . As a result, in common practice, a QCD multijet event with large  $E_T^{\text{miss}}$  caused by a jet  $p_T$  overestimate will not be rejected either.

In Refs. [14–17], CMS used the angular variable  $\Delta\varphi_{\text{min}}^*$ , the minimum of the angles  $\Delta\varphi_i^*$  of all jets in the event, where  $\Delta\varphi_i^*$  denotes the azimuthal angle between a jet  $i$  and the negative vector sum of  $\vec{p}_T$  of all *other* jets in the event. The angular variable  $\Delta\varphi_{\text{min}}^*$  first appeared in Refs. [18, 19] and was used to identify large  $E_T^{\text{miss}}$  caused by masked regions of the calorimeter [15].<sup>1</sup> In recent results [14, 16, 17],  $\Delta\varphi_{\text{min}}^*$  was used, along with

<sup>1</sup>In Ref. [18],  $\Delta\varphi_{\text{min}}^*$  is referred to as “biased”  $\Delta\phi$ . In Refs. [15, 19],  $\Delta\varphi_{\text{min}}^*$  is denoted by  $\Delta\phi^*$ .

another dimensionless variable  $\alpha_T$  [15, 20], to suppress QCD multijet background events to a negligible level; events were required to have  $\Delta\varphi_{\min}^*$  above a threshold,  $\Delta\varphi_{\min}^* \geq \gamma_0$  (the  $\Delta\varphi_{\min}^*$  criterion), with  $\gamma_0 = 0.3$  in Ref. [16] and 0.5 in Refs. [14, 17].

The  $\Delta\varphi_{\min}^*$  criterion can reject QCD multijet background events with large  $E_T^{\text{miss}}$  caused by a jet  $p_T$  overestimate or by an underestimate even when the jet whose  $p_T$  is underestimated is not among the highest  $p_T$  jets in the event. The  $\Delta\varphi_{\min}^*$  criterion can reject QCD multijet background events to a negligible level while still keeping signal acceptances of SUSY models large enough to carry out the search. However, the  $\Delta\varphi_{\min}^*$  criterion does largely reduce signal acceptances, in particular of models with high jet multiplicity.<sup>2</sup>

In this paper, after reviewing the angle  $\Delta\varphi_i^*$  and the  $\Delta\varphi_{\min}^*$  criterion, we introduce three alternative angular variables:  $\tilde{\omega}_{\min}$ ,  $\hat{\omega}_{\min}$ , and  $\chi_{\min}$ . These variables are designed to maintain good signal acceptances of SUSY models, in particular of models with high jet multiplicity in the final state, while rejecting QCD multijet background events to a negligible level. Receiver operating characteristic (ROC) curves in simulated event samples demonstrate that  $\hat{\omega}_{\min}$  and  $\chi_{\min}$  considerably outperform  $\Delta\varphi_{\min}^*$  and  $\Delta\varphi_i$  in rejecting QCD multijet background events and that  $\hat{\omega}_{\min}$  and  $\tilde{\omega}_{\min}$  are also useful for reducing the total standard model background events.

This paper proceeds as follows. Section 2 reviews the angle  $\Delta\varphi_i^*$ . In Section 3, we determine the minimized  $H_T^{\text{miss}}$  in the variation of jet  $p_T$  and show the relation of the minimized  $H_T^{\text{miss}}$  to the angle  $\Delta\varphi_i^*$ . Section 4 describes simulated event samples. In Section 5, we show that the minimized  $H_T^{\text{miss}}$  for the jet that is mismeasured or has neutrinos from hadron decays is small in QCD multijet events in the simulated event samples. Section 6 reviews features of the  $\Delta\varphi_{\min}^*$  criterion and identifies room for improvement. The three alternative angular variables,  $\tilde{\omega}_{\min}$ ,  $\hat{\omega}_{\min}$ , and  $\chi_{\min}$ , are introduced in Section 7. Section 8 demonstrates the performance of these variables in the simulated event samples. A summary is given in Section 9.

## 2 Review of angle $\Delta\varphi_i^*$

In this section, after providing the definitions of kinematic variables, including  $\Delta\varphi_i^*$ , as used in this paper, we show that  $\Delta\varphi_i^*$  can be written as a function of two dimensionless variables and review the properties of  $\Delta\varphi_i^*$ .

### 2.1 Definitions

**Missing transverse hadronic momentum  $\vec{H}_T^{\text{miss}}$ .** The missing transverse hadronic momentum ( $\vec{H}_T^{\text{miss}}$ ) is the negative vector sum of  $\vec{p}_T$  of all jets in the event:

$$\vec{H}_T^{\text{miss}} \equiv - \sum_{i \in \text{jets}} \vec{p}_{Ti}. \quad (2.1)$$

Its magnitude is denoted by  $H_T^{\text{miss}}$ . The two vectors  $\vec{E}_T^{\text{miss}}$  and  $\vec{H}_T^{\text{miss}}$  have similar values in all-hadronic final states. In this paper, we focus on all-hadronic final states and primarily

---

<sup>2</sup>See, for example, the additional tables 7-11 of [17], which can be found at <http://cms-results.web.cern.ch/cms-results/public-results/publications/SUS-15-005/index.html>.

use  $\vec{H}_T^{\text{miss}}$ . However, much of the discussion in this paper is valid even if  $\vec{H}_T^{\text{miss}}$  is replaced with  $\vec{E}_T^{\text{miss}}$ .

**Angle  $\Delta\varphi_i$ .** The angle  $\Delta\varphi_i$  is the angle between the  $\vec{p}_T$  of jet  $i$  and  $\vec{H}_T^{\text{miss}}$ :

$$\Delta\varphi_i \equiv \Delta\varphi(\vec{p}_{Ti}, \vec{H}_T^{\text{miss}}). \quad (2.2)$$

The angle  $\Delta\varphi_i$  ranges from 0 to  $\pi$ . This angle is often defined with  $\vec{E}_T^{\text{miss}}$  instead of  $\vec{H}_T^{\text{miss}}$ . Both definitions have similar values in all-hadronic final states. We define  $\Delta\varphi_i$  with  $\vec{H}_T^{\text{miss}}$  as in Eq. (2.2) in this paper.

We let  $\vec{H}_{Ti}^{\text{miss}*}$  denote the vector sum of  $\vec{H}_T^{\text{miss}}$  and the jet  $\vec{p}_{Ti}$ :

$$\vec{H}_{Ti}^{\text{miss}*} \equiv \vec{H}_T^{\text{miss}} + \vec{p}_{Ti} = - \sum_{j \in \text{jets}} \vec{p}_{Tj} + \vec{p}_{Ti} = - \sum_{\substack{j \in \text{jets} \\ j \neq i}} \vec{p}_{Tj}. \quad (2.3)$$

It is the negative vector sum of  $\vec{p}_T$  of all jets but the jet  $i$  in the event. Its magnitude is denoted by  $H_{Ti}^{\text{miss}*}$ .

**Angle  $\Delta\varphi_i^*$ .** The angle  $\Delta\varphi_i^*$  is the angle between the jet  $\vec{p}_{Ti}$  and  $\vec{H}_{Ti}^{\text{miss}*}$ :

$$\Delta\varphi_i^* \equiv \Delta\varphi(\vec{p}_{Ti}, \vec{H}_{Ti}^{\text{miss}*}) = \Delta\varphi(\vec{p}_{Ti}, \vec{H}_T^{\text{miss}} + \vec{p}_{Ti}). \quad (2.4)$$

The angle  $\Delta\varphi_i^*$  ranges from 0 to  $\pi$ . In the  $\vec{E}_T^{\text{miss}}$ -based definition, this angle can be defined as the angle between the jet  $\vec{p}_{Ti}$  and the vector sum  $\vec{E}_T^{\text{miss}} + \vec{p}_{Ti}$ . In this paper we define  $\Delta\varphi_i^*$  with  $\vec{H}_T^{\text{miss}}$  as in Eq. (2.4).

## 2.2 Geometric relations

Since  $\Delta\varphi_i^*$  is the angle between the jet  $\vec{p}_{Ti}$  and  $\vec{H}_{Ti}^{\text{miss}*}$ , its cosine is

$$\cos \Delta\varphi_i^* = \frac{\vec{p}_{Ti} \cdot (\vec{H}_T^{\text{miss}} + \vec{p}_{Ti})}{|\vec{p}_{Ti}| |\vec{H}_T^{\text{miss}} + \vec{p}_{Ti}|},$$

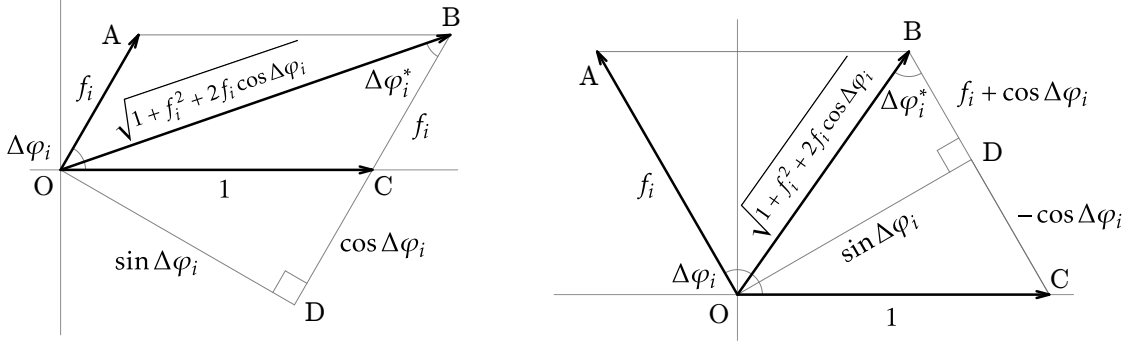
which can be written as

$$\cos \Delta\varphi_i^* = \frac{f_i + \cos \Delta\varphi_i}{\sqrt{1 + f_i^2 + 2f_i \cos \Delta\varphi_i}}, \quad (2.5)$$

where  $f_i$  is the ratio of the magnitudes of  $\vec{p}_{Ti}$  and  $\vec{H}_T^{\text{miss}}$ :

$$f_i \equiv \frac{p_{Ti}}{H_T^{\text{miss}}}. \quad (2.6)$$

This ratio plays a key role in this paper. In Eq. (2.5),  $\Delta\varphi_i^*$  is written as a function of two dimensionless variables,  $\Delta\varphi_i$  and  $f_i$ . Figure 1 depicts the geometric relations among  $\Delta\varphi_i^*$ ,  $\Delta\varphi_i$ , and  $f_i$  in the transverse momentum ( $p_x$ - $p_y$ ) plane that is normalized as follows.



(a)  $\Delta\varphi_i < \pi/2$ , a near side jet.

(b)  $\Delta\varphi_i > \pi/2$ , an away side jet.

**Figure 1:** The geometric relations among  $\Delta\varphi_i^*$ ,  $\Delta\varphi_i$ , and  $f_i$  in the normalized  $p_T$  plane, the transverse momentum plane that is rotated and scaled such that  $\vec{H}_T^{\text{miss}}$  points horizontally to the right with unit length and that is flipped if necessary so that  $\Delta\varphi_i$  lies between 0 and  $\pi$ . The vectors  $\vec{OA}$ ,  $\vec{OB}$ , and  $\vec{OC}$  are the jet  $\vec{p}_{Ti}$ ,  $\vec{H}_{Ti}^{\text{miss}*}$ , and  $\vec{H}_T^{\text{miss}}$ , respectively. The point D is the projection of the point O onto the line BC.

**Normalized  $p_T$  plane.** The *normalized  $p_T$  plane*—the coordinate plane in Fig. 1—is the transverse momentum plane that is rotated and scaled such that the vector  $\vec{H}_T^{\text{miss}}$  points horizontally to the right with unit length. Moreover, the plane is flipped if necessary so that  $\Delta\varphi_i$  lies between 0 and  $\pi$ . The unit vector  $\vec{OC}$  is  $\vec{H}_T^{\text{miss}}$  in this plane. The vector  $\vec{OA}$ , with the length  $f_i$ , is the jet  $\vec{p}_{Ti}$ . The angle  $\angle AOC$  is, therefore, the angle  $\Delta\varphi_i$ . The normalized  $p_T$  plane is used throughout in this paper.

**Near side, away side.** If the angle  $\Delta\varphi_i$  is an acute angle, the jet is in the *near side* of  $\vec{H}_T^{\text{miss}}$  (Fig. 1a)—the jet is a near side jet; if the angle  $\Delta\varphi_i$  is an obtuse angle, the jet is in the *away side* of  $\vec{H}_T^{\text{miss}}$  (Fig. 1b)—the jet is an away side jet.

The vector  $\vec{OB}$  is  $\vec{H}_{Ti}^{\text{miss}*}$ . The length OB is  $H_{Ti}^{\text{miss}*}$  in the scale of this plane:

$$\begin{aligned} |\vec{OB}| &= \sqrt{1 + f_i^2 + 2f_i \cos \Delta\varphi_i} \\ &= \frac{\sin \Delta\varphi_i}{\sin \Delta\varphi_i^*} \quad (\text{unless } \Delta\varphi_i \text{ is } 0 \text{ or } \pi). \end{aligned} \quad (2.7)$$

The angle  $\angle AOB$  is  $\Delta\varphi_i^*$ , and so is its alternate angle  $\angle OBC$  as shown in Fig. 1.

### 2.3 Analytic properties

Equation (2.5) relates  $\Delta\varphi_i^*$  to  $\Delta\varphi_i$  and  $f_i$ . The angle  $\Delta\varphi_i^*$  is plotted in Fig. 2 as a function of  $\Delta\varphi_i$  for different values of  $f_i$ . The angle  $\Delta\varphi_i^*$  is never wider than  $\Delta\varphi_i$ . The angle  $\Delta\varphi_i^*$  is zero when  $\Delta\varphi_i$  is zero for any values of  $f_i$ . In the limit of  $f_i \rightarrow 0$ ,  $\Delta\varphi_i^*$  is the same as  $\Delta\varphi_i$  in the entire range from 0 to  $\pi$ . For any given value of  $\Delta\varphi_i$ , the larger the ratio  $f_i$ , the narrower the angle  $\Delta\varphi_i^*$ . If  $f_i < 1$ ,  $\Delta\varphi_i^*$  is wider than half the angle  $\Delta\varphi_i$  and is the same

as  $\Delta\varphi_i$  at  $\pi$ . If  $f_i = 1$ ,  $\Delta\varphi_i^*$  is half the angle  $\Delta\varphi_i$  except when  $\Delta\varphi_i = \pi$ , at which  $\Delta\varphi_i^*$  is indeterminate.<sup>3</sup> If  $f_i > 1$ ,  $\Delta\varphi_i^*$  is narrower than half the angle  $\Delta\varphi_i$  and is zero when  $\Delta\varphi_i$  is  $\pi$ . As  $f_i$  approaches infinity,  $\Delta\varphi_i^*$  converges to zero for any values of  $\Delta\varphi_i$ .

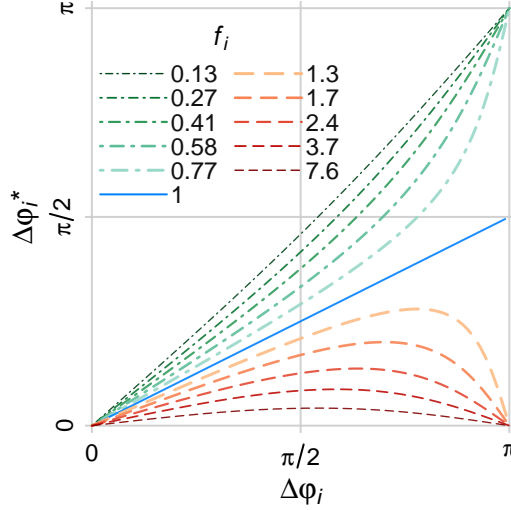


**Figure 2:** The angle  $\Delta\varphi_i^*$  as a function of the angle  $\Delta\varphi_i$  for different values of  $f_i$ .

### 3 Minimizing $H_T^{\text{miss}}$ by varying jet $p_T$

A jet mismeasurement or neutrinos in hadron decays in a jet can largely alter the magnitude of the jet  $\vec{p}_T$  from that of the “true” jet  $\vec{p}_T$  (which we loosely define as the jet  $\vec{p}_T$  at the hadron level, before leptonic or semileptonic decays). However, normally, the direction of the jet  $\vec{p}_T$  is not largely altered. Therefore, if we vary the magnitude of  $\vec{p}_T$  of the jet that is mismeasured or has neutrinos from hadron decays while retaining its direction, the jet  $\vec{p}_T$  becomes at some point in the variation close to the “true” jet  $\vec{p}_T$ .

Consequently, if large  $H_T^{\text{miss}}$  in a QCD multijet event is caused by a jet mismeasurement or neutrinos in hadron decays in a jet, it will be possible to make  $H_T^{\text{miss}}$  small by varying the  $p_T$  of one of the jets in the event. In contrast, it is not generally possible to make large genuine  $H_T^{\text{miss}}$  in a signal event small by varying the  $p_T$  of any of the jets in the event.

In this section, we consider the variation of the magnitude of the jet  $\vec{p}_{T_i}$  and determine the minimized  $H_T^{\text{miss}}$  in the variation. The range of the variation that we consider is from zero to infinity rather than a range comparable to the jet  $p_T$  resolution because large  $H_T^{\text{miss}}$  can be caused by a *substantial* jet mismeasurement or *high- $p_T$*  neutrinos in hadron decays. At the end of the section, we show the relation of the minimized  $H_T^{\text{miss}}$  to the angle  $\Delta\varphi_i^*$ . In Section 5, we will demonstrate that the minimized  $H_T^{\text{miss}}$  for the jet that is mismeasured

<sup>3</sup> If  $f_i = 1$  and  $\Delta\varphi_i = \pi$ ,  $\Delta\varphi_i^*$  is indeterminate because then  $\vec{H}_{T_i}^{\text{miss}*}$  is a zero vector, which is always the case for the jets in monojet events. If  $f_i = 1$ , as  $\Delta\varphi_i$  approaches  $\pi$ ,  $\Delta\varphi_i^*$  approaches  $\pi/2$ . It is, therefore, sensible and convenient to define  $\Delta\varphi_i^*|_{\Delta\varphi_i=\pi, f_i=1} \equiv \pi/2$ .





By definition,  $\vec{H}_{T_i}^{\text{miss}*}$  does not change in the variation because its value is determined by the other jets in the event—the vector  $\vec{OB}$  is always  $\vec{H}_{T_i}^{\text{miss}*}$ . Thus, Eq. (3.1) makes it clear how  $\vec{H}_T^{\text{miss}}$  changes when the magnitude of  $\vec{p}_{T_i}$  is varied. If  $f_i + \cos \Delta\varphi_i \geq 0$ , the vectors  $\vec{OD}$  and  $\vec{DB}$  are, respectively, the minimized  $\vec{H}_T^{\text{miss}}$  and the minimizing jet  $\vec{p}_{T_i}$  (Fig. 3a); if  $f_i + \cos \Delta\varphi_i < 0$ , the vector  $\vec{OB}$  is the minimized  $\vec{H}_T^{\text{miss}}$ , and the minimizing jet  $\vec{p}_{T_i}$  is a zero vector  $\vec{0}$  (Fig. 3b).

### 3.2 Scale factor $\sin \Delta\tilde{\varphi}_i$ and ratio $g_i$

We have determined the two vectors in the normalized  $p_T$  plane: the minimized  $\vec{H}_T^{\text{miss}}$  and the minimizing jet  $\vec{p}_{T_i}$ . Here, we will introduce two dimensionless quantities—the scale factor  $\sin \Delta\tilde{\varphi}_i$  and the ratio  $g_i$ —to denote the two vectors' magnitudes in the scale of the normalized  $p_T$  plane.

**Scale factor  $\sin \Delta\tilde{\varphi}_i$ .** The scale factor  $\sin \Delta\tilde{\varphi}_i$  is the minimized  $H_T^{\text{miss}}$  in the scale of the normalized  $p_T$  plane, which is the length OD if  $f_i + \cos \Delta\varphi_i \geq 0$  and the length OB (Eq. (2.7)) otherwise<sup>4</sup>:

$$\begin{aligned} \sin \Delta\tilde{\varphi}_i &\equiv \begin{cases} \sin \Delta\varphi_i & \text{if } f_i + \cos \Delta\varphi_i \geq 0 \\ \sqrt{1 + f_i^2 + 2f_i \cos \Delta\varphi_i} & \text{otherwise.} \end{cases} \\ &= \sqrt{1 + (\min(f_i, -\cos \Delta\varphi_i))^2 + 2 \min(f_i, -\cos \Delta\varphi_i) \cos \Delta\varphi_i} \end{aligned} \quad (3.2)$$

In other words,  $\sin \Delta\tilde{\varphi}_i$  is the factor by which  $H_T^{\text{miss}}$  is scaled from its initial value when it is minimized in the variation of the jet  $p_{T_i}$ .

The scale factor  $\sin \Delta\tilde{\varphi}_i$  is plotted in Fig. 4 as a function of  $\Delta\varphi_i$  for different values of  $f_i$ . The scale factor  $\sin \Delta\tilde{\varphi}_i$  is larger than  $\sin \Delta\varphi_i$  if  $f_i + \cos \Delta\varphi_i < 0$ , that is, if  $\vec{OB}$  is the minimized  $\vec{H}_T^{\text{miss}}$  in the normalized  $p_T$  plane as in Fig. 3b.

**Ratio  $g_i$ .** The ratio  $g_i$  is the minimizing jet  $p_{T_i}$  in the scale of the normalized  $p_T$  plane, which is the length BD if  $f_i + \cos \Delta\varphi_i \geq 0$  and is zero otherwise:

$$\begin{aligned} g_i &\equiv \begin{cases} f_i + \cos \Delta\varphi_i & \text{if } f_i + \cos \Delta\varphi_i \geq 0 \\ 0 & \text{otherwise} \end{cases} \\ &= \max(f_i + \cos \Delta\varphi_i, 0). \end{aligned} \quad (3.3)$$

As a result,  $g_i$  is the ratio of the minimizing jet  $p_{T_i}$  and the initial  $H_T^{\text{miss}}$ .

---

<sup>4</sup>In this paper, the angle  $\Delta\tilde{\varphi}_i$  always appears in the sine function. The angle  $\Delta\tilde{\varphi}_i$  itself can be defined as

$$\Delta\tilde{\varphi}_i \equiv \begin{cases} \Delta\varphi_i & \text{if } f_i + \cos \Delta\varphi_i \geq 0 \\ \pi - \arcsin(\sqrt{1 + f_i^2 + 2f_i \cos \Delta\varphi_i}) & \text{otherwise.} \end{cases}$$

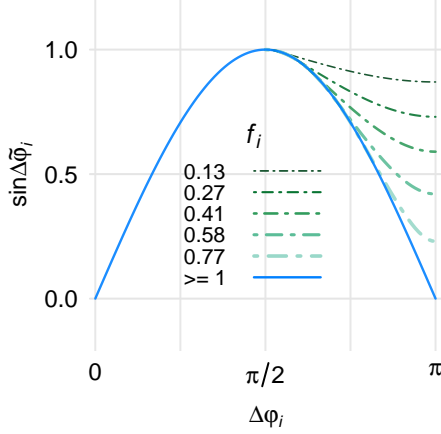


**Figure 4:** The scale factor  $\sin \Delta\tilde{\varphi}_i$  as a function of  $\Delta\varphi_i$  for different values of  $f_i$ .

**Minimized  $H_T^{\text{miss}}$  and minimizing jet  $p_{Ti}$ .** In terms of  $\sin \Delta\tilde{\varphi}_i$  and  $g_i$ , the minimized  $H_T^{\text{miss}}$  and the minimizing jet  $p_{Ti}$  are

$$\begin{aligned} \text{minimized } H_T^{\text{miss}} &= H_T^{\text{miss}} \sin \Delta\tilde{\varphi}_i \\ \text{minimizing jet } p_{Ti} &= g_i H_T^{\text{miss}}, \end{aligned} \quad (3.4)$$

where  $H_T^{\text{miss}}$  in the right-hand side is the initial  $H_T^{\text{miss}}$ .

### 3.3 Relation to angle $\Delta\varphi_i^*$

We have determined the minimized  $H_T^{\text{miss}}$  as well as the minimizing jet  $p_{Ti}$ . Before closing this section, we point out their relation to the angle  $\Delta\varphi_i^*$ . The ratio of minimized  $H_T^{\text{miss}}$  and the minimizing jet  $p_{Ti}$  is

$$\frac{\text{minimized } H_T^{\text{miss}}}{\text{minimizing jet } p_{Ti}} = \frac{\sin \Delta\tilde{\varphi}_i}{g_i} = \begin{cases} \frac{\sin \Delta\varphi_i}{f_i + \cos \Delta\varphi_i} & \text{if } f_i + \cos \Delta\varphi_i \geq 0 \\ \infty & \text{otherwise.} \end{cases} \quad (3.5)$$

From Eq. (2.5),  $\tan \Delta\varphi_i^*$  can be written as

$$\tan \Delta\varphi_i^* = \frac{\sin \Delta\varphi_i}{f_i + \cos \Delta\varphi_i}, \quad (3.6)$$

which is the same as the ratio for the case of  $f_i + \cos \Delta\varphi_i \geq 0$  in Eq. (3.5). Therefore, in words, the relation is that  $\tan \Delta\varphi_i^*$  is the ratio of the minimized  $H_T^{\text{miss}}$  and minimizing jet  $p_{Ti}$  provided  $f_i + \cos \Delta\varphi_i \geq 0$ . In Sections 7, we will define alternative angles based on similar relations.

We started this section by arguing that it is possible to make large  $H_T^{\text{miss}}$  in a QCD multijet event small by varying the  $p_T$  of one of the jets in the event. We then determined

the minimized  $H_T^{\text{miss}}$  in the variation of a jet  $p_T$ . The minimized  $H_T^{\text{miss}}$  can be defined for each jet in the event. In Section 5, we will show that the minimum of the minimized  $H_T^{\text{miss}}$  for all jets in a QCD multijet event with large  $H_T^{\text{miss}}$  is indeed generally small in simulated event samples, which will be described in the next section.

## 4 Simulated event samples

We have generated Monte Carlo simulated events of proton-proton collisions at  $\sqrt{s} = 13$  TeV. This section describes the simulated event samples.

**MadGraph5+Pythia8.** Events were generated at the parton level at leading order with MADGRAPH5\_aMC@NLO 2.3.3 [21] with the parton distribution function NNPDF2.3 LO [22]. The fragmentation and parton shower were simulated by PYTHIA 8.2 [23] with the MLM matching [24].

**Background processes.** We generated events for the following standard model processes as background samples.

**QCD.** QCD multijet events were generated with up to three outgoing partons in the matrix element calculation of MADGRAPH5\_aMC@NLO.<sup>5</sup>

**EWK.** In this paper,  $t\bar{t}$ +jets,  $W$ +jets, and  $Z(\rightarrow \nu\bar{\nu})$ +jets events are collectively called EWK events, as done for example in Ref. [15]. Apart from QCD multijet events, these processes are typical dominant background processes in all-hadronic SUSY searches as for example in Refs. [1, 10]. The  $t\bar{t}$ +jets events were generated with up to three additional outgoing partons. MADSPIN [25] was used for the top quark decay in the  $t\bar{t}$ +jets events. The  $W$ +jets and  $Z(\rightarrow \nu\bar{\nu})$ +jets events were generated with up to four additional outgoing partons.

**Signal processes.** As benchmark signal models, we generated events in two models from a class of simplified SUSY models [26, 27] in which gluinos are produced in pairs and each gluino decays into a top-antitop quark pair and a neutralino as the LSP ( $\tilde{g} \rightarrow t\bar{t}\tilde{\chi}_1^0$ ). This class of models is called T1tttt in CMS [28] and Gtt in ATLAS [29]. Models are fully specified when the gluino mass  $m_{\tilde{g}}$  and the neutralino mass  $m_{\tilde{\chi}_1^0}$  are specified. We picked two pairs of the masses and refer the two signal models as follows:

**T1tttt(1950, 500).**  $m_{\tilde{g}} = 1950$  GeV and  $m_{\tilde{\chi}_1^0} = 500$  GeV, a *high-mass gluino model* with large split between  $m_{\tilde{g}}$  and  $m_{\tilde{\chi}_1^0}$ .

**T1tttt(1350, 1100).**  $m_{\tilde{g}} = 1350$  GeV and  $m_{\tilde{\chi}_1^0} = 1000$  GeV, a *compressed spectrum*, in which the difference between  $m_{\tilde{g}}$  and  $m_{\tilde{\chi}_1^0}$  is small.

These mass pairs are near the exclusion contour in the  $m_{\tilde{g}}-m_{\tilde{\chi}_1^0}$  plane in this class of the models in recent CMS and ATLAS results [1, 2, 5, 9, 10, 14, 30–34]. The events were generated with up to two additional outgoing partons.

---

<sup>5</sup>We compared with a small sample generated with up to four outgoing partons and observed agreement in distributions of the leading jet  $p_T$ , the inclusive jet  $p_T$ , the jet multiplicity,  $H_T$ ,  $H_T^{\text{miss}}$ , and  $E_T^{\text{miss}}$ .

**Delphes with CMS card.** The detector responses to the events were simulated by DELPHES 3.4.1 [35] with the CMS detector configuration card. We used the configuration file `delphes_card_CMS_PileUp.tcl` included in the DELPHES package with a slight modification.<sup>6</sup>

On average, 23 pileup interactions were placed in each event by DELPHES. Further, DELPHES performed (a) the reconstruction of physics objects such as jets, electrons, muons, photons, and missing transverse momentum; (b) the calculations of the isolation variables for electrons, muons, and photons; (c) the  $\tau$  tagging of jets; and (d) pileup subtraction on jets.

**Jets, generated jets, jet  $p_T$  correction.** Jets were defined by the anti- $k_T$  algorithm [36] with the distance parameter 0.4 by FASTJET [37, 38] within DELPHES. In addition, *generated* jets as sets of particles after the fragmentation, parton shower, and decay of certain short-lived particles were defined also by the anti- $k_T$  algorithm with the distance parameter 0.4 by FASTJET within DELPHES. Generated jets do not include neutrinos or neutralinos.

The jet transverse momenta  $p_T$  were corrected such that the peak locations of the distributions of jet  $p_T$  agreed with those for the generated jet  $p_T$  in ranges of  $p_T$  and the pseudorapidity ( $\eta$ ). Jets with  $p_T \geq 30$  GeV were used. The jet  $p_T$  resolution is shown in Appendix C.

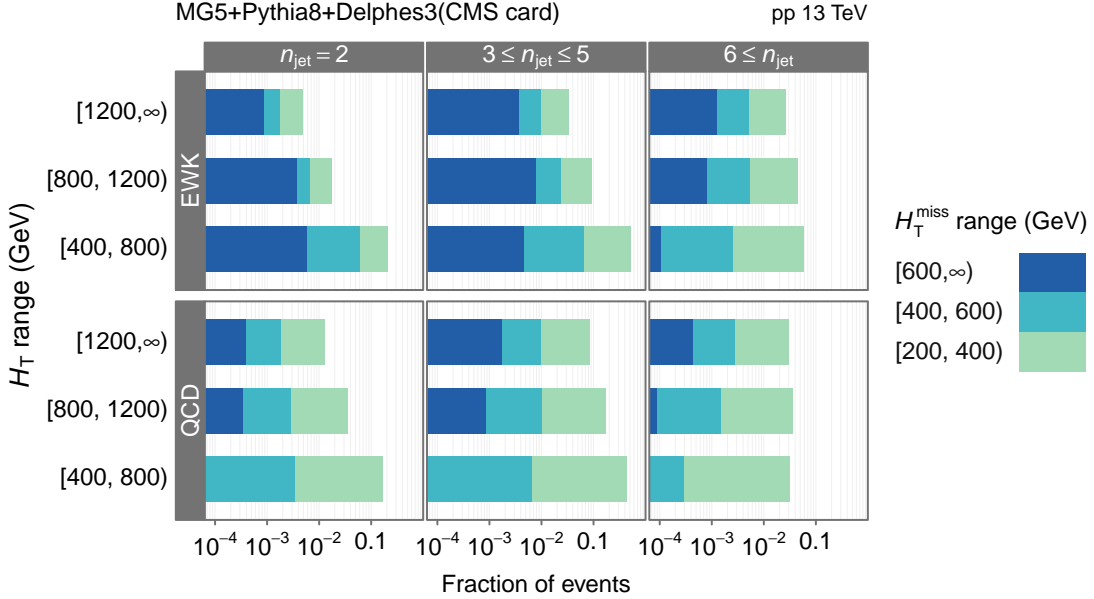


**Figure 5:** The fractions of the events in ranges of  $n_{\text{jet}}$ ,  $H_T$ , and  $H_T^{\text{miss}}$  for the background processes after the event selection is applied. The fractions add up to unity separately for the QCD and EWK events.

<sup>6</sup>We changed the average number of pileup interactions and the distance parameter of the anti- $k_T$  algorithm and excluded neutralinos from generated jets.

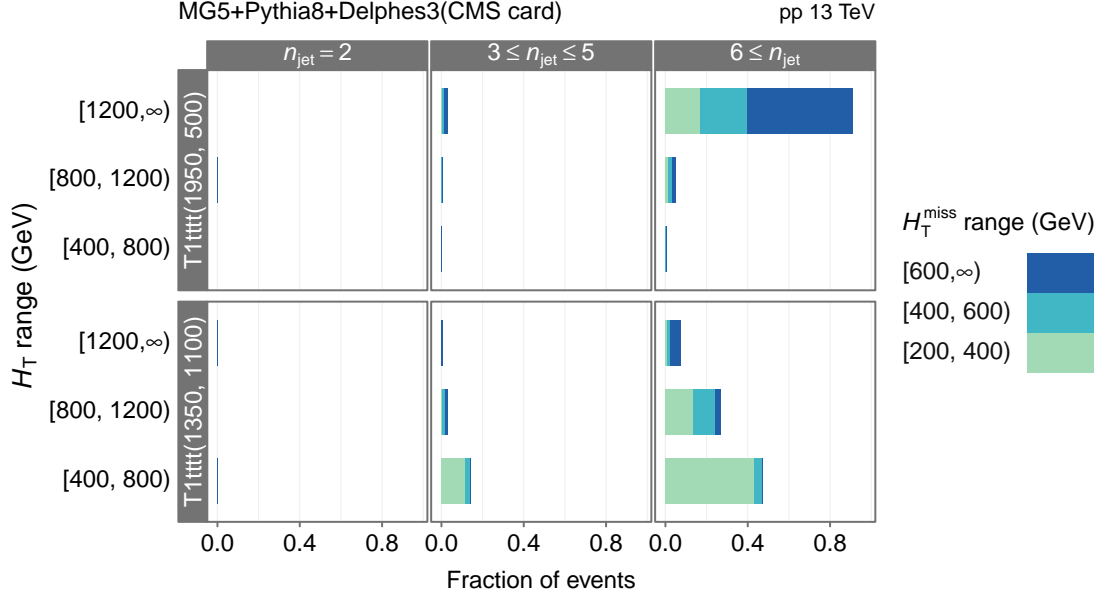


**Figure 6:** The fractions of the events in ranges of  $n_{\text{jet}}$ ,  $H_T$ , and  $H_T^{\text{miss}}$  for the two signal models, T1tttt(1950, 500) and T1tttt(1350, 1100), after the event selection is applied. The fractions add up to unity separately for each model.

**Event selection.** Events with any of at least one isolated electron, isolated muon, or isolated photon, were discarded. Events were discarded if they contain a jet that did not satisfy quality criteria<sup>7</sup> or that was tagged as hadronically decaying  $\tau$ .

Events were required (a) to have at least two jets ( $n_{\text{jet}} \geq 2$ ); (b) to satisfy  $H_T \geq 400$  GeV where  $H_T$  is the scalar sum of  $p_T$  of all jets in the event; (c) to have large  $H_T^{\text{miss}}$ , namely,  $H_T^{\text{miss}} \geq 200$  GeV; and (d) to satisfy  $H_T^{\text{miss}}/E_T^{\text{miss}} < 1.25$ , which, as used for example in Ref. [17], ensures that the large  $H_T^{\text{miss}}$  is not due to unclustered objects or jets with  $p_T$  below the threshold of 30 GeV.

The fractions of the selected events in ranges of  $n_{\text{jet}}$ ,  $H_T$ , and  $H_T^{\text{miss}}$  for the QCD and EWK events are shown in Fig. 5 and for the two signal models in Fig. 6. High jet multiplicity events ( $n_{\text{jet}} \geq 6$ ) dominate for both signal models. Most events in T1tttt(1950, 500) are in the highest- $H_T$  range. A large fraction of events in T1tttt(1350, 1100) have low to medium  $H_T$  and low  $H_T^{\text{miss}}$ .

## 5 Minimized $H_T^{\text{miss}}$ in QCD multijet events

At the beginning of Section 3, we argued that the minimized  $H_T^{\text{miss}}$  in the variation of  $p_T$  of one of the jets in a QCD multijet event with large  $H_T^{\text{miss}}$  should be small as long as the large  $H_T^{\text{miss}}$  is caused by a jet mismeasurement or neutrinos in hadron decays in a jet, while in

<sup>7</sup>In terms of variables in DELPHES, the criteria are  $\text{Beta} \geq 0.14$ ,  $\text{NCharged} > 0$ ,  $\text{PTD} < 0.8$ , and  $\text{MeanSqDeltaR} < 0.1$ .

a signal event the minimized  $H_T^{\text{miss}}$  is not necessarily small for any of the jets in the event. In the simulated event samples just described in the previous section, this section confirms the argument.

We let  $\tilde{H}_{T\text{min}}^{\text{miss}}$  denote the minimum among the minimized  $H_T^{\text{miss}}$  for all jets in the event:

$$\tilde{H}_{T\text{min}}^{\text{miss}} \equiv H_T^{\text{miss}} \min_{i \in \text{jets}} \sin \Delta\tilde{\varphi}_i, \quad (5.1)$$

where  $\sin \Delta\tilde{\varphi}_i$  is defined in Eq. (3.2).

Figure 7 shows that, in the simulated event samples, the distribution of QCD multijet events in  $\tilde{H}_{T\text{min}}^{\text{miss}}$  quickly decreases by orders of magnitude while the distributions in  $\tilde{H}_{T\text{min}}^{\text{miss}}$  for the other processes decrease more slowly:  $\tilde{H}_{T\text{min}}^{\text{miss}}$  is indeed generally small in QCD events with large  $H_T^{\text{miss}}$ . Moreover, the figure also shows that, in QCD multijet events,  $\tilde{H}_{T\text{min}}^{\text{miss}}$  roughly agrees with “true”  $H_T^{\text{miss}}$ , which is estimated by the magnitude of the vector sum of  $\vec{p}_T$  of the generated jets and the neutrinos within  $\Delta R = \sqrt{\Delta\varphi^2 + \Delta\eta^2} \leq 0.4$  from the axis of any of the generated jets.

The small  $\tilde{H}_{T\text{min}}^{\text{miss}}$  in QCD multijet events with large  $H_T^{\text{miss}}$  and its rough agreement with the “true”  $H_T^{\text{miss}}$  indicate (a) that the large  $H_T^{\text{miss}}$  in QCD multijet events is in fact dominantly caused by a jet mismeasurement and neutrinos in hadron decays in a jet and (b) that, in QCD multijet events with large  $H_T^{\text{miss}}$ , the minimizing  $p_T$  for the jet that yields  $\tilde{H}_{T\text{min}}^{\text{miss}}$  is in fact close to the “true” jet  $p_T$ .

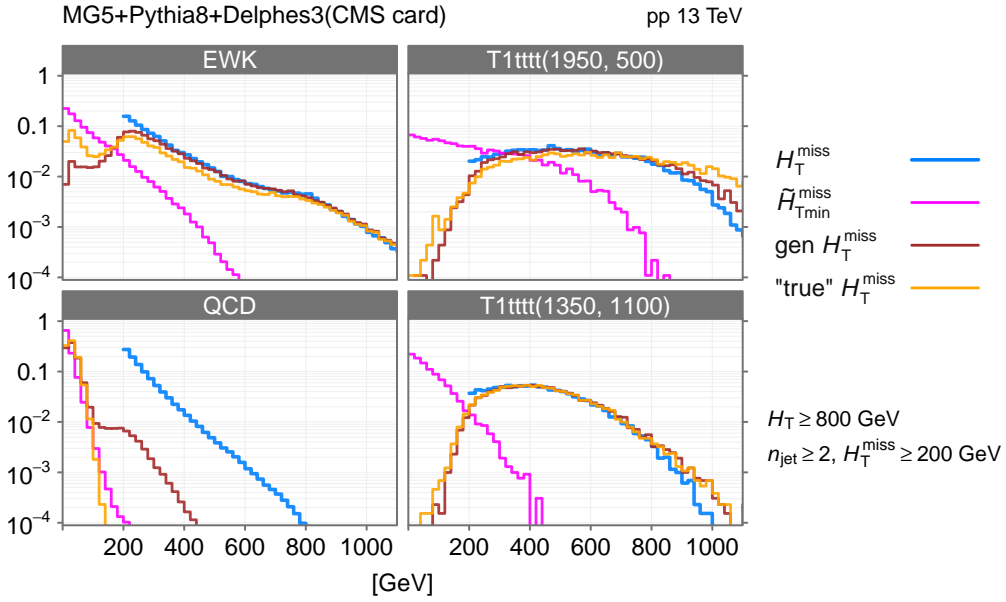


**Figure 7:** The distributions of QCD, EWK, T1tttt(1350, 1100), and T1tttt(1950, 500) events in  $H_T^{\text{miss}}$  and three related variables:  $\tilde{H}_{T\text{min}}^{\text{miss}}$ , defined in Eq. (5.1); the  $\text{gen } H_T^{\text{miss}}$ , the  $H_T^{\text{miss}}$  based on generated jets, which do not include neutrinos; the “true”  $H_T^{\text{miss}}$ , the  $H_T^{\text{miss}}$  based on the generated jets including the neutrinos within  $\Delta R = \sqrt{\Delta\varphi^2 + \Delta\eta^2} \leq 0.4$  from the axis of any of the generated jets. Each distribution is normalized to unity.

This short section has confirmed the argument made at the beginning of Section 3 in simulated event samples. This confirmation suggests that  $\tilde{H}_{\text{Tmin}}^{\text{miss}}$  can possibly replace  $H_{\text{T}}^{\text{miss}}$  (or  $E_{\text{T}}^{\text{miss}}$ ) in the event selection, which is pursued in Appendix A.

## 6 Features of $\Delta\varphi_{\text{min}}^*$ criterion

This section reviews the features of the  $\Delta\varphi_{\text{min}}^*$  criterion. Let us first restate the definitions of the angular variable  $\Delta\varphi_{\text{min}}^*$  and the  $\Delta\varphi_{\text{min}}^*$  criterion.

**Angular variable  $\Delta\varphi_{\text{min}}^*$ .** The angular variable  $\Delta\varphi_{\text{min}}^*$  is the minimum of the angles  $\Delta\varphi_i^*$ , defined in (2.4), for all jets in the event:

$$\Delta\varphi_{\text{min}}^* \equiv \min_{i \in \text{jets}} \Delta\varphi_i^*. \quad (6.1)$$

**The  $\Delta\varphi_{\text{min}}^*$  criterion.** The  $\Delta\varphi_{\text{min}}^*$  criterion of the event selection requires events to have  $\Delta\varphi_{\text{min}}^*$  above a threshold  $\gamma_0$ :

$$\Delta\varphi_{\text{min}}^* \geq \gamma_0. \quad (6.2)$$

In other words, the  $\Delta\varphi_{\text{min}}^*$  criterion rejects any event with at least one jet with the angle  $\Delta\varphi_i^*$  narrower than  $\gamma_0$ . The value of  $\gamma_0$  is 0.5 in Refs. [14, 17]. The discussion in this section is not valid if  $\gamma_0$  is too large, for example, as large as  $\pi/2 \approx 1.57$  or larger.

Section 2.3 reviewed the properties of  $\Delta\varphi_i^*$  as a function of  $\Delta\varphi_i$  and  $f_i$ . Here, we will relate the properties with features of the  $\Delta\varphi_{\text{min}}^*$  criterion. In particular, we consider large  $f_i$ , wide  $\Delta\varphi_i$ , and narrow  $\Delta\varphi_i$  and identify room for improvement.

### 6.1 Large $f_i$ and $f_{\text{max}}$

When  $f_i$  is larger than unity,  $\Delta\varphi_i^*$  is not an increasing function of  $\Delta\varphi_i$  as can be seen in Fig. 2. From Eq. (2.5),  $\Delta\varphi_i^*$  takes its maximum value of  $\arcsin(1/f_i)$  when  $\cos \Delta\varphi_i = -1/f_i$ . For example, since  $1/\sin \gamma_0|_{\gamma_0=0.5} = 2.09$ , the  $\Delta\varphi_{\text{min}}^*$  criterion with  $\gamma_0 = 0.5$  rejects any event with a jet with  $p_{\text{T}}$  at least 2.09 times as large as  $H_{\text{T}}^{\text{miss}}$ .

In general, the  $\Delta\varphi_{\text{min}}^*$  criterion rejects all events with

$$f_{\text{max}} \equiv \max_{i \in \text{jets}} f_i \geq \frac{1}{\sin \gamma_0}. \quad (6.3)$$

This feature might appear to needlessly reduce signal acceptances; on the contrary, it effectively reduces background events without much decreasing signal acceptances. In fact, the distributions of QCD and EWK background events in  $f_{\text{max}}$  have the peaks at larger values than those of signal events, as shown in Fig. 8.<sup>8</sup>

---

<sup>8</sup>The variable  $f_{\text{max}}$  could, therefore, be useful for offline and online preselection of events for reducing data sizes and event rates.

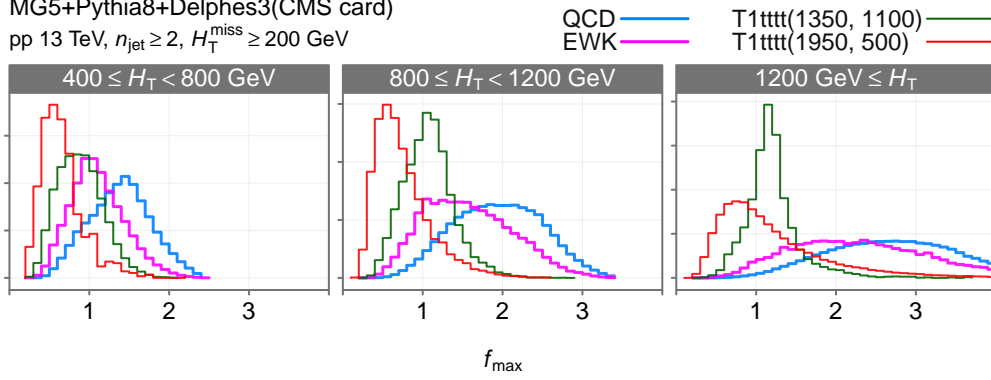


**Figure 8:** The distributions of QCD, EWK, T1tttt(1950, 500), and T1tttt(1350, 1100) events in  $f_{\max}$  in three ranges of  $H_T$  in the simulated samples described in Section 4. Each distribution is normalized to unity.

## 6.2 Wide $\Delta\varphi_i$ and jet $p_T$ overestimate

Consider wide  $\Delta\varphi_i$  (near  $\pi$ ). The jet and  $\vec{H}_T^{\text{miss}}$  are back-to-back. As can be seen in Fig. 2, when  $\Delta\varphi_i$  is near  $\pi$ ,  $\Delta\varphi_i^*$  will be below the threshold  $\gamma_0$  only if  $f_i > 1$ . Consequently, the  $\Delta\varphi_{\min}^*$  criterion rejects every event with a jet back-to-back with  $\vec{H}_T^{\text{miss}}$  if the jet  $p_T$  is greater than  $H_T^{\text{miss}}$ , whereas the criterion does not reject any event with a jet back-to-back with  $\vec{H}_T^{\text{miss}}$  if the jet  $p_T$  is less than  $H_T^{\text{miss}}$  unless another jet in the same event has narrow  $\Delta\varphi_i^*$ . This difference based on whether the jet  $p_T$  is greater or less than  $H_T^{\text{miss}}$  is an advantage in rejecting QCD multijet background events with large  $H_T^{\text{miss}}$  caused by a jet  $p_T$  overestimate.

If a jet  $p_T$  overestimate causes large  $H_T^{\text{miss}}$ , the jet and  $\vec{H}_T^{\text{miss}}$  are back-to-back and the jet  $p_T$  is greater than  $H_T^{\text{miss}}$ . The reason why the jet  $p_T$  is greater than  $H_T^{\text{miss}}$  is that  $H_T^{\text{miss}}$  corresponds only to the amount by which the jet  $p_T$  is overestimated. An example is illustrated in Fig. 9. In contrast, in signal events where large  $H_T^{\text{miss}}$  is due to invisible particles, a jet back-to-back with  $\vec{H}_T^{\text{miss}}$  does not necessarily have  $p_T$  greater than  $H_T^{\text{miss}}$ . A simple example is given in Fig. 10.

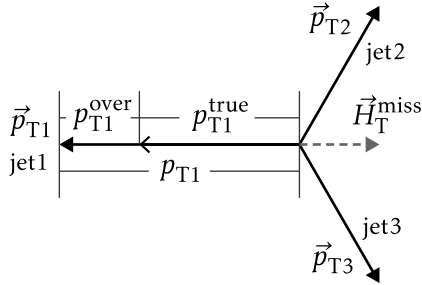


**Figure 9:** Schematic illustrating when a jet  $p_T$  overestimate causes large  $H_T^{\text{miss}}$  in a QCD event, the jet  $\vec{p}_T$  and  $\vec{H}_T^{\text{miss}}$  are back-to-back and the jet  $p_T$  is greater than  $H_T^{\text{miss}}$ . The jet  $p_{T1}$ , with its true value  $p_{T1}^{\text{true}}$ , is overestimated by  $p_{T1}^{\text{over}}$ , which causes  $\vec{H}_T^{\text{miss}}$ . The  $H_T^{\text{miss}}$  corresponds to the amount by which  $p_{T1}$  is overestimated, i.e.,  $H_T^{\text{miss}} = p_{T1}^{\text{over}}$ ; therefore,  $p_{T1} > H_T^{\text{miss}}$ .



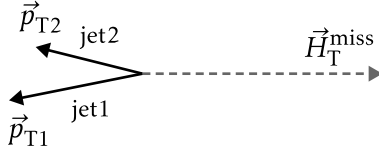


**Figure 10:** A simple example of signal events where jets back-to-back with  $\vec{H}_T^{\text{miss}}$  have each  $p_T$  smaller than  $H_T^{\text{miss}}$ . Because the two jets share the recoil of  $\vec{H}_T^{\text{miss}}$ , each jet has  $p_{Ti}$  ( $i = 1, 2$ ) smaller than  $H_T^{\text{miss}}$ .

### 6.3 Narrow $\Delta\varphi_i$ —room for improvement

Consider narrow  $\Delta\varphi_i$ . If large  $H_T^{\text{miss}}$  in a QCD multijet event is caused by a jet  $p_T$  *underestimate*, which can be due to either a mismeasurement or neutrinos in hadron decays, the jet has narrow  $\Delta\varphi_i$ . Because  $\Delta\varphi_i^*$  is always narrow when  $\Delta\varphi_i$  is narrow, the  $\Delta\varphi_{\text{min}}^*$  criterion rejects QCD multijet background events with large  $H_T^{\text{miss}}$  caused by a jet  $p_T$  underestimate.

As a function of  $\Delta\varphi_i$  and  $f_i$ ,  $\Delta\varphi_i^*$  is larger for smaller  $f_i$  for a given value of  $\Delta\varphi_i$  (Fig. 2). Therefore, the  $\Delta\varphi_{\text{min}}^*$  criterion, in effect, lowers the threshold on  $\Delta\varphi_i$  of a jet with smaller  $f_i$ . This is advantageous because, in a QCD multijet event with large  $H_T^{\text{miss}}$  caused by a jet  $p_T$  underestimate,  $\Delta\varphi_i$  of the jet whose  $p_T$  is underestimated tends to be narrower if its  $f_i$  is smaller. The reason is as follows: the smaller  $f_i$  indicates that a larger fraction of the “true” jet  $p_T$  contributes to  $H_T^{\text{miss}}$ , aligning  $\vec{H}_T^{\text{miss}}$  more with the “true” jet  $\vec{p}_T$ , which in turn results in narrower  $\Delta\varphi_i$ , as long as the jet  $\vec{p}_{Ti}$  is parallel to the “true” jet  $\vec{p}_T$ .<sup>9</sup>

However, because  $\Delta\varphi_i^*$  is never wider than  $\Delta\varphi_i$  by definition, the effective threshold of  $\Delta\varphi_i$  is never lower than  $\gamma_0$ . Consequently, the  $\Delta\varphi_{\text{min}}^*$  criterion rejects every event with at least one jet with  $\Delta\varphi_i < \gamma_0$ . This feature needlessly reduces signal acceptances, especially of models with high jet multiplicity, such as T1tttt, the benchmark signal models used in this paper. There is room for improvement here. For example, it is possible to keep signal acceptances larger if the effective threshold of  $\Delta\varphi_i$  can be arbitrarily low for sufficiently small  $f_i$ . Angular variables with such a property will be introduced in the next section.

## 7 Alternative angular variables: $\tilde{\omega}_{\text{min}}$ , $\hat{\omega}_{\text{min}}$ , $\chi_{\text{min}}$

In the previous section, we have reviewed the features of the  $\Delta\varphi_{\text{min}}^*$  criterion and identified room for improvement. In this section, we introduce three alternative angular variables— $\tilde{\omega}_{\text{min}}$ ,  $\hat{\omega}_{\text{min}}$ , and  $\chi_{\text{min}}$ —after introducing the angle  $\omega_i$  and its three variants  $\tilde{\omega}_i$ ,  $\hat{\omega}_i$ , and  $\chi_i$ .

### 7.1 Angle $\omega_i$

The angle  $\omega_i$  brings the improvement for near side jets mentioned at the end of the previous section. However,  $\omega_i$  loses the advantage of  $\Delta\varphi_i^*$  for away side jets described in Section 6.2. Later, we will introduce three variants of  $\omega_i$  that recover the lost advantage.

<sup>9</sup>In general, the jet  $\vec{p}_{Ti}$  is not exactly parallel to the “true” jet  $\vec{p}_T$ . In fact, the larger the underestimate, the more deflected the jet  $\vec{p}_T$  is likely to be from the direction of the “true” jet  $\vec{p}_T$ . This is a minor counter effect to the described relation between  $\Delta\varphi_i$  and  $f_i$ .

We saw in Section 3.3 that  $\tan \Delta\varphi_i^*$  is the ratio of the minimized  $H_T^{\text{miss}}$  and the minimizing jet  $p_{Ti}$  as long as  $f_i + \cos \Delta\varphi_i \geq 0$ . The tangent of the angle  $\omega_i$  is a similar ratio.

**Angle  $\omega_i$ .** The angle  $\omega_i$  is defined such that  $\tan \omega_i$  is the ratio of  $\sin \Delta\varphi_i$  and  $f_i$ :

$$\tan \omega_i \equiv \frac{\sin \Delta\varphi_i}{f_i}. \quad (7.1)$$

The angle  $\omega_i$  ranges in  $0 \leq \omega_i < \pi/2$ . The  $\tan \omega_i$  is the ratio of the minimized  $H_T^{\text{miss}}$  and the initial jet  $p_{Ti}$  if  $f_i + \cos \Delta\varphi_i \geq 0$ .

**Geometric relations.** The angle  $\omega_i$  appears in the normalized  $p_T$  plane as shown in Fig. 11: the angle  $\angle OAD$  is  $\omega_i$ . The angle  $\omega_i$  is wider than  $\Delta\varphi_i^*$  for a near side jet (Fig. 11a) and is narrower than  $\Delta\varphi_i^*$  for an away side jet (Figs. 11b). If  $\Delta\varphi_i = \pi/2$ , the two angles are the same.

**As function of  $\Delta\varphi_i$  and  $f_i$ .** The angle  $\omega_i$  is plotted as a function of  $\Delta\varphi_i$  for different values of  $f_i$  in Fig. 12. The function is symmetric around  $\Delta\varphi_i = \pi/2$ , at which it takes its maximum value of  $\text{arccot } f_i$ . The angle  $\omega_i$  is zero when  $\Delta\varphi_i$  is zero or  $\pi$ . The smaller the ratio  $f_i$ , the more quickly the angle  $\omega_i$  increases from zero near  $\Delta\varphi_i = 0$  and decreases to zero near  $\Delta\varphi_i = \pi$ . In the limit of  $f_i \rightarrow 0$ ,  $\omega_i$  becomes a step function of  $\Delta\varphi_i$  that jumps from zero to  $\pi/2$  at  $\Delta\varphi_i = 0$  and from  $\pi/2$  to zero at  $\Delta\varphi_i = \pi$ .

**Improvement for near side jets.** The improvement for near side jets discussed in Section 6.3 can be seen in Fig. 12. The angle  $\omega_i$  can be wider than  $\Delta\varphi_i$  for near side jets. In fact, no matter how narrow the angle  $\Delta\varphi_i$  is (except 0),  $\omega_i$  can be wider than any given acute angle if  $f_i$  is sufficiently small. Furthermore, no matter how small the ratio  $f_i$  is,  $\omega_i$  can be narrower than any given angle if  $\Delta\varphi_i$  is sufficiently small. These properties let the

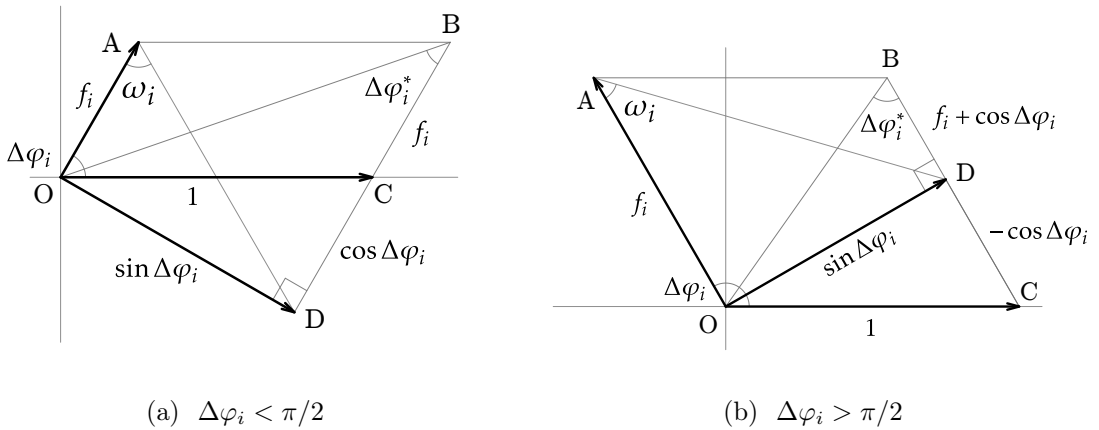


**Figure 11:** The angle  $\omega_i$  in the normalized  $p_T$  plane, where  $\vec{OC}$  and  $\vec{OA}$  are  $\vec{H}_T^{\text{miss}}$  and the jet  $\vec{p}_{Ti}$ , respectively. The angle  $\angle OAD$  is the angle  $\omega_i$ .

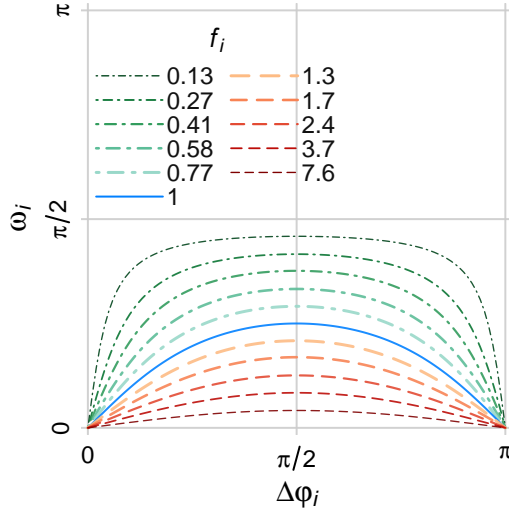


**Figure 12:** The angle  $\omega_i$  as a function of the angle  $\Delta\varphi_i$  for different values of  $f_i$ .

near side jets whose  $p_T$  are underestimated in QCD multijet events with large  $H_T^{\text{miss}}$  have narrow  $\omega_i$  while preventing any near side jet in signal events from unnecessarily having narrow  $\omega_i$ .

**Lost advantage for away side jets.** The angle  $\omega_i$  does not have the advantage of  $\Delta\varphi_i^*$  for away side jets described in Section 6.2: the angle  $\omega_i$  is zero at  $\Delta\varphi_i = \pi$  regardless of whether  $f_i$  is greater or less than unity. This property makes the angles  $\omega_i$  of jets in signal events unnecessarily narrow if the jets have  $p_T$  less than  $H_T^{\text{miss}}$  and are back-to-back with  $\vec{H}_T^{\text{miss}}$ .

## 7.2 Variants of $\omega_i$

We introduce three variants of the angle  $\omega_i$  to recover the lost advantage. These variants, denoted by  $\tilde{\omega}_i$ ,  $\hat{\omega}_i$ , and  $\chi_i$ , have the same value as  $\omega_i$  for near side jets but can be wider than  $\omega_i$  for away side jets.

### 7.2.1 Angle $\tilde{\omega}_i$

The  $\tan \omega_i$  is the ratio of the minimized  $H_T^{\text{miss}}$  and the initial jet  $p_{T_i}$  only if  $f_i + \cos \Delta\varphi_i \geq 0$ . The first variant, denoted by  $\tilde{\omega}_i$ , is defined such that its tangent is always the ratio regardless of the sign of the sum  $f_i + \cos \Delta\varphi_i$ .

**Angle  $\tilde{\omega}_i$ .** The angle  $\tilde{\omega}_i$  is defined such that  $\tan \tilde{\omega}_i$  is the ratio of  $\sin \Delta\tilde{\varphi}_i$  and  $f_i$ :

$$\tan \tilde{\omega}_i \equiv \frac{\sin \Delta\tilde{\varphi}_i}{f_i}, \quad (7.2)$$

where  $\sin \Delta\tilde{\varphi}_i$  is the scale factor defined in Eq. (3.2). The angle  $\tilde{\omega}_i$  ranges in  $0 \leq \tilde{\omega}_i < \pi/2$ .

Compared to  $\tan \omega_i$  in Eq. (7.1),  $\sin \Delta\varphi_i$  in the numerator is replaced with  $\sin \Delta\tilde{\varphi}_i$ . The angle  $\tilde{\omega}_i$  is plotted as a function of  $\Delta\varphi_i$  for different values of  $f_i$  in the leftmost panel of Fig. 13. The angle  $\tilde{\omega}_i$  is wider than  $\omega_i$  if  $f_i + \cos \Delta\varphi_i < 0$  and is not zero at  $\Delta\varphi_i = \pi$  if  $f_i < 1$ .

### 7.2.2 Angle $\hat{\omega}_i$

Consider the minimized  $H_T^{\text{miss}}$  in the variation of  $p_{T_i}$  of only near side jets. The minimized  $H_T^{\text{miss}}$  in such variation can be expressed as the following scale factor.

**Scale factor  $\sin \Delta\hat{\varphi}_i$ .** The scale factor  $\sin \Delta\hat{\varphi}_i$  is defined as

$$\sin \Delta\hat{\varphi}_i \equiv \begin{cases} \sin \Delta\varphi_i & \text{if } \Delta\varphi_i \leq \pi/2 \\ 1 & \text{otherwise.} \end{cases} \quad (7.3)$$

The angle  $\Delta\hat{\varphi}_i$  can be written as  $\Delta\hat{\varphi}_i = \min(\Delta\varphi_i, \pi/2)$ .

This scale factor is motivated by considering event topologies where all jets in the event are away side jets, which are unlike topologies for QCD multijet events and possible topologies for signal events. QCD multijet events usually have both near and away side jets. With this scale factor,  $H_T^{\text{miss}}$  is not minimized if the event has only away side jets. When large  $H_T^{\text{miss}}$  in QCD multijet events is caused by a jet  $p_{T_i}$  overestimate, the variation of the jet  $p_{T_i}$  that is actually overestimated is not considered. But the variation of  $p_{T_i}$  of near side jets in the same event can still minimize  $H_T^{\text{miss}}$  to some extent.

**Angle  $\hat{\omega}_i$ .** The angle  $\hat{\omega}_i$  is defined such that  $\tan \hat{\omega}_i$  is the ratio of  $\sin \Delta\hat{\varphi}_i$  and  $f_i$ :

$$\tan \hat{\omega}_i \equiv \frac{\sin \Delta\hat{\varphi}_i}{f_i}. \quad (7.4)$$

The angle  $\hat{\omega}_i$  ranges in  $0 \leq \hat{\omega}_i < \pi/2$ . The  $\tan \hat{\omega}_i$  is the ratio of the minimized (initial)  $H_T^{\text{miss}}$  and the initial jet  $p_{T_i}$  for near (away) side jets.

The angle  $\hat{\omega}_i$  is plotted as a function of  $\Delta\varphi_i$  for different values of  $f_i$  in the middle panel of Fig. 13. The angle  $\hat{\omega}_i$  is the same as  $\omega_i$  for near side jets. For away side jets,  $\hat{\omega}_i$  does not depend on  $\Delta\varphi_i$  and its value is  $\text{arccot } f_i$ . The angle  $\hat{\omega}_i$  is the same as or wider than  $\tilde{\omega}_i$ .

### 7.2.3 Angle $\chi_i$

The last variant  $\chi_i$  is a combination of  $\omega_i$  and  $\Delta\varphi_i^*$ .

**Ratio  $k_i$ .** The ratio  $k_i$  is defined as

$$k_i \equiv \min(f_i, g_i) = \begin{cases} f_i & \text{if } \Delta\varphi_i \leq \pi/2 \\ g_i & \text{otherwise,} \end{cases} \quad (7.5)$$

where  $g_i$  is defined in Eq. (3.3). The ratio  $k_i$  is the ratio of the initial (minimizing) jet  $p_{T_i}$  and the initial  $H_T^{\text{miss}}$  for near (away) side jets.

**Angle  $\chi_i$ .** The angle  $\chi_i$  is defined such that  $\tan \chi_i$  is the ratio of  $\sin \Delta \tilde{\varphi}_i$  and  $k_i$ <sup>10</sup>:

$$\tan \chi_i \equiv \frac{\sin \Delta \tilde{\varphi}_i}{k_i}. \quad (7.6)$$

The angle  $\chi_i$  ranges from 0 to  $\pi/2$ . The  $\tan \chi_i$  is the ratio of minimized  $H_T^{\text{miss}}$  and the initial (minimizing) jet  $p_{Ti}$  for near (away) side jets.

In the rightmost panel of Fig. 13, the angle  $\chi_i$  is shown as a function of  $\Delta \varphi_i$  for different values of  $f_i$ . It is not smooth at  $\Delta \varphi_i = \pi/2$ , but continuous. The angle  $\chi_i$  is the same as  $\omega_i$  for near side jets and is the same as  $\Delta \varphi_i^*$  for away side jets except  $\chi_i$  is capped at  $\pi/2$ . The angle  $\chi_i$  has the advantage of  $\omega_i$  for near side jets and of  $\Delta \varphi_i^*$  for away side jets.

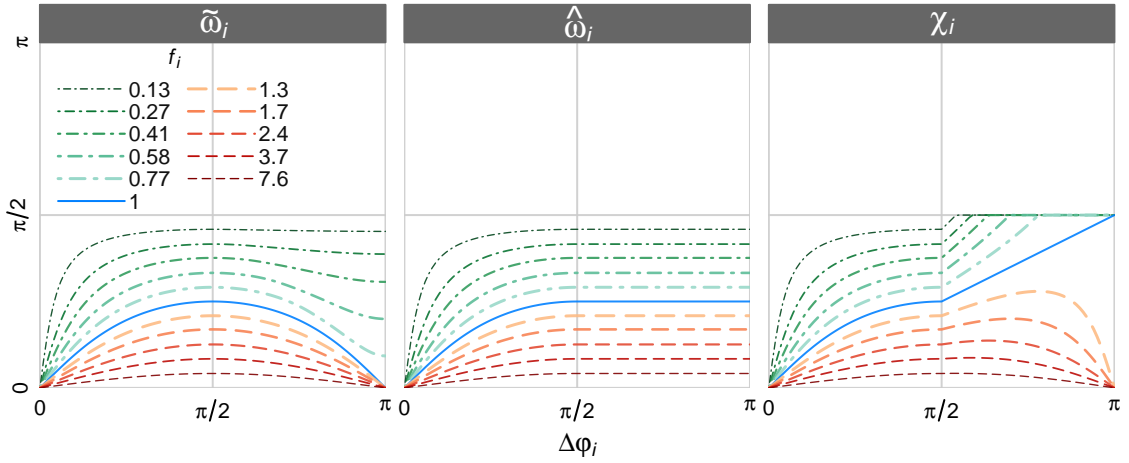


**Figure 13:** The angles  $\tilde{\omega}_i$ ,  $\hat{\omega}_i$ , and  $\chi_i$  as a function of  $\Delta \varphi_i$  for different values of  $f_i$ .

### 7.3 Alternative angular variables: $\tilde{\omega}_{\min}$ , $\hat{\omega}_{\min}$ , $\chi_{\min}$

Finally, we introduce the alternative angular variables. The three variants of  $\omega_i$  can be defined for each jet. The alternative angular variables, to be defined for each event, are the minima of these angles for all jets in the event:

$$\tilde{\omega}_{\min} \equiv \min_{i \in \text{jets}} \tilde{\omega}_i \quad (7.7)$$

$$\hat{\omega}_{\min} \equiv \min_{i \in \text{jets}} \hat{\omega}_i \quad (7.8)$$

$$\chi_{\min} \equiv \min_{i \in \text{jets}} \chi_i. \quad (7.9)$$

The angles  $\tilde{\omega}_i$ ,  $\hat{\omega}_i$ , and  $\chi_i$  are defined as their tangents, respectively, in Eqs. (7.2), (7.4), and (7.6). There, the angles are defined in terms of various scale factors and ratios defined throughout the paper, such as  $\sin \Delta \tilde{\varphi}_i$ ,  $\sin \Delta \hat{\varphi}_i$ ,  $g_i$ , and  $k_i$ .

<sup>10</sup>As is the case for  $\Delta \varphi_i^*$ ,  $\chi_i$  is indeterminate if  $f_i = 1$  and  $\Delta \varphi_i = \pi$  and can be defined as  $\pi/2$ .

Here, for convenience, we write down these angles in terms of only  $\Delta\varphi_i$  and  $f_i$ :

$$\tilde{\omega}_i = \arctan \left( \frac{\sqrt{1 + (\min(f_i, -\cos \Delta\varphi_i))^2 + 2 \min(f_i, -\cos \Delta\varphi_i) \cos \Delta\varphi_i}}{f_i} \right), \quad (7.10)$$

$$\hat{\omega}_i = \arctan \left( \frac{\sin(\min(\Delta\varphi_i, \pi/2))}{f_i} \right), \quad (7.11)$$

$$\chi_i = \arctan \left( \frac{\sqrt{1 + (\min(f_i, -\cos \Delta\varphi_i))^2 + 2 \min(f_i, -\cos \Delta\varphi_i) \cos \Delta\varphi_i}}{\min(f_i, \max(f_i + \cos \Delta\varphi_i, 0))} \right). \quad (7.12)$$

The numerators of all three fractions in the arguments of  $\arctan$  range in  $[0, 1]$ . The denominators for  $\tilde{\omega}_i$  and  $\hat{\omega}_i$  are positive, that is,  $f_i > 0$ . The denominator for  $\chi_i$  is zero or positive. The angles  $\tilde{\omega}_i$  and  $\hat{\omega}_i$  range in  $[0, \pi/2)$ . The angle  $\chi_i$  ranges in  $[0, \pi/2]$ .

## 8 Performance in simulated events

This section compares, in the simulated event samples described in Section 4, the performances of the three alternative angular variables introduced in the previous section and two conventional variables. The two conventional variables are  $\Delta\varphi_{\min}^*$ , which we reviewed in detail in Section 6, and  $\Delta\varphi_{\min 4}$ , which is defined as the minimum of the angles  $\Delta\varphi_i$  of up to four highest  $p_T$  jets in the event:

$$\Delta\varphi_{\min 4} \equiv \min_{i \in \{1, \dots, \min(4, n_{\text{jet}})\}} \Delta\varphi_i. \quad (8.1)$$

We picked  $\Delta\varphi_{\min 4}$  as the benchmark event variable of  $\Delta\varphi_i$  for the performance comparison. The  $\Delta\varphi_{\min 4}$  (with  $\Delta\varphi_i$  defined with  $\vec{E}_T^{\text{miss}}$ ) was used, for example, in Refs. [2, 3, 10].

The values of the five variables,  $\Delta\varphi_{\min 4}$ ,  $\Delta\varphi_{\min}^*$ ,  $\tilde{\omega}_{\min}$ ,  $\hat{\omega}_{\min}$ , and  $\chi_{\min}$ , for the same event have the following relations by definition:

$$\tilde{\omega}_{\min} \leq \hat{\omega}_{\min} \quad (8.2)$$

$$\tilde{\omega}_{\min} \leq \chi_{\min} \quad (8.3)$$

$$\min(\Delta\varphi_{\min}^*, \pi/2) \leq \chi_{\min} \quad (8.4)$$

$$\Delta\varphi_{\min}^* \leq \Delta\varphi_{\min 4}. \quad (8.5)$$

### Event distributions

Figure 14 shows the event distributions of the background and signal processes in the five variables. Each distribution is normalized to unity. By definition,  $\chi_{\min}$ ,  $\tilde{\omega}_{\min}$ , and  $\hat{\omega}_{\min}$  range from zero to  $\pi/2$ , whereas  $\Delta\varphi_{\min 4}$  and  $\Delta\varphi_{\min}^*$  range from zero to  $\pi$ .

In all variables, the distributions of QCD multijet events have the maximum at zero and quickly decrease roughly exponentially by orders of magnitude, whereas the distributions of events for the other processes are generally more spread. QCD multijet background events can be, therefore, rejected by applying a threshold on one of these variables.

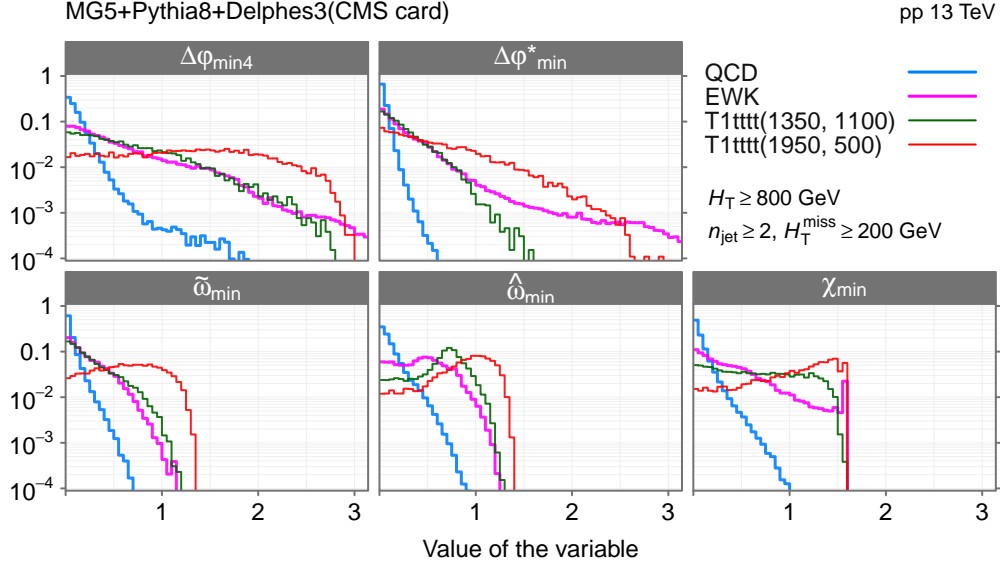


**Figure 14:** The distributions of QCD, EWK, T1tttt(1950, 500), and T1tttt(1350, 1100) events in the conventional variables ( $\Delta\varphi_{\min 4}$ ,  $\Delta\varphi_{\min}^*$ ) and the alternative variables ( $\tilde{\omega}_{\min}$ ,  $\hat{\omega}_{\min}$ , and  $\chi_{\min}$ ). Each distribution is normalized to unity.

The distribution of the QCD multijet events in  $\chi_{\min}$  decreases more slowly than that in  $\Delta\varphi_{\min}^*$ , which is unavoidable because of the relation Eq. (8.4). The advantage of  $\chi_{\min}$  over  $\Delta\varphi_{\min}^*$  is that, despite the high jet multiplicity, the distribution of the signal events are roughly uniform, which can be attributed to the improvement of  $\omega_i$  for near side jets described in Section 7.1.

The distributions of EWK and signal events in  $\hat{\omega}_{\min}$  have maxima at larger values. These maxima appear because the value of  $\hat{\omega}_i$  is close to  $\text{arccot } f_i$  except for narrow  $\Delta\varphi_i$  as we saw in Section 7.2.2. Because  $\text{arccot } f_i$  is a decreasing function of  $f_i$ , the order of the processes for which these maxima appear, i.e., EWK, T1tttt(1350, 1100), and T1tttt(1950, 500), corresponds to the reverse order of the processes for which the maxima of the distributions in  $f_{\max}$  appear (Fig. 8).

The distribution of the T1tttt(1950, 500) events in  $\tilde{\omega}_{\min}$  has a maximum at a larger value while the distributions of the T1tttt(1350, 1100) and EWK events have a maximum at zero. This is because the maximum of the  $f_{\max}$  distribution of the T1tttt(1950, 500) events is less than unity but those for T1tttt(1350, 1100) and EWK are greater than unity (Fig. 8).

The EWK events are distributed in the entire ranges of  $\Delta\varphi_{\min 4}$ ,  $\Delta\varphi_{\min}^*$ , and  $\Delta\varphi_{\min}^*$ , but not of  $\tilde{\omega}_{\min}$  or  $\hat{\omega}_{\min}$ . In  $\tilde{\omega}_{\min}$  and  $\hat{\omega}_{\min}$ , the distributions of the EWK events decrease somewhat more quickly than the distribution of the T1tttt(1350, 1100) events and much more quickly than the distribution of the T1tttt(1950, 500). EWK events can be, therefore, also reduced by applying a threshold on  $\tilde{\omega}_{\min}$  or  $\hat{\omega}_{\min}$ .

## ROC curves

The ROC curves in Fig. 15 demonstrate in the simulated event samples that the alternative variables  $\hat{\omega}_{\min}$  and  $\chi_{\min}$  outperform the conventional variables  $\Delta\varphi_{\min 4}$  and  $\Delta\varphi_{\min}^*$  in rejecting QCD multijet background events and that the alternative variables  $\hat{\omega}_{\min}$  and  $\tilde{\omega}_{\min}$  are useful for reducing the total standard model background events.

Figure 15a shows the ROC curves against the selection efficiency of the QCD multijet background events. The alternative variables  $\hat{\omega}_{\min}$  and  $\chi_{\min}$  considerably outperform the conventional variables for a wide range of the efficiency for both signal models in all  $H_T$  ranges. For example, at the same selection efficiency of the QCD multijet events with  $\Delta\varphi_{\min}^* \geq 0.5$ ,  $\chi_{\min}$  can improve the signal efficiency for T1tttt(1950, 500) by 9% for the lowest  $H_T$  range, 18% for the medium  $H_T$  range, and 4% for the highest  $H_T$  range and for T1tttt(1350, 1100), 15%, 20%, and 12% respectively in each  $H_T$  range.

The alternative variable  $\tilde{\omega}_{\min}$  performs, for T1tttt(1950, 500), nearly as well as  $\hat{\omega}_{\min}$  in the lowest  $H_T$  range, but only as well as  $\Delta\varphi_{\min}^*$  for the two highest  $H_T$  ranges. For T1tttt(1350, 1100),  $\tilde{\omega}_{\min}$  performs well only for the tight background rejection in the lowest  $H_T$  range.

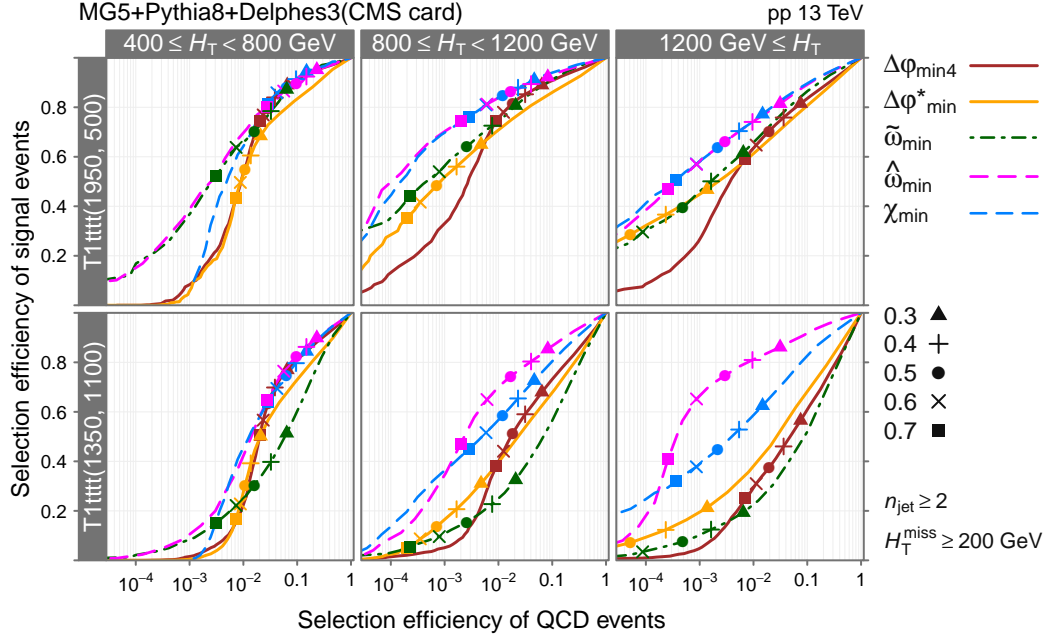
Figure 15b shows similar ROC curves but against the selection efficiency of the total standard model (QCD+EWK) background events. Here  $\hat{\omega}_{\min}$ , overall, performs the best among the five variables. At the same selection efficiency of the background events with  $\Delta\varphi_{\min}^* \geq 0.5$ ,  $\hat{\omega}_{\min}$  can improve the signal efficiency for T1tttt(1950, 500) by 21% for the lowest  $H_T$  range, 25% for the medium  $H_T$  range, and 18% for the highest  $H_T$  range and for T1tttt(1350, 1100), 24%, 30%, and 32% respectively in each  $H_T$  range. The variable  $\tilde{\omega}_{\min}$  performs nearly as well as  $\hat{\omega}_{\min}$  for tight background rejection in all  $H_T$  ranges for T1tttt(1950, 500). For T1tttt(1350, 1100),  $\tilde{\omega}_{\min}$  performs well only for the tight background rejection in the lowest  $H_T$  range.

## 9 Summary

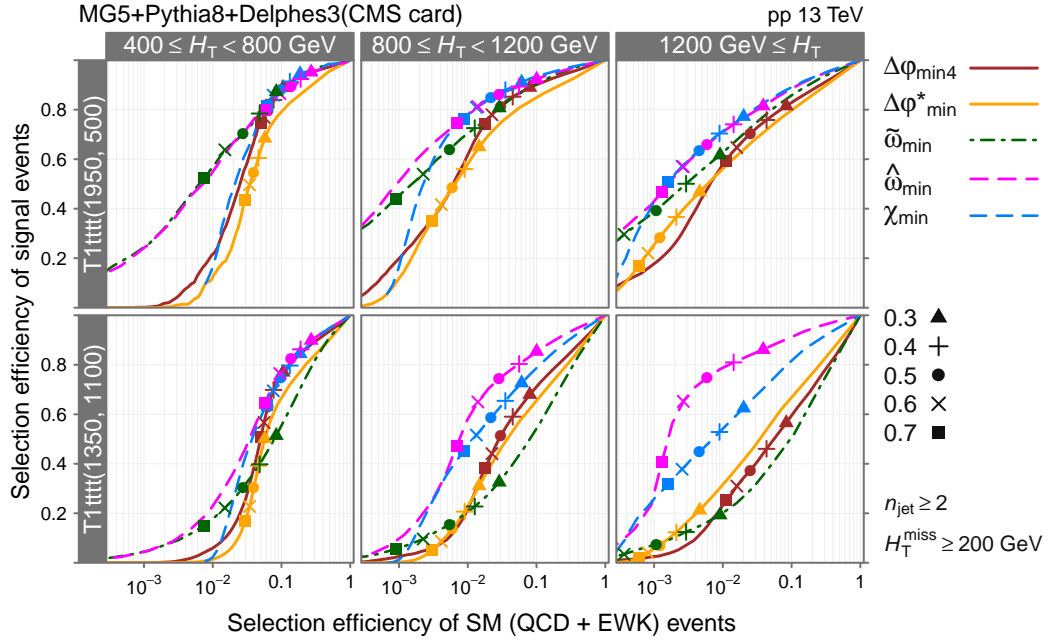
We introduced three angular variables— $\tilde{\omega}_{\min}$ ,  $\hat{\omega}_{\min}$ , and  $\chi_{\min}$ —as alternatives to  $\Delta\varphi_{\min}^*$  as well as to  $\Delta\varphi_i$  for QCD multijet background event suppression in SUSY searches in all-hadronic final states in proton-proton collisions at the LHC. We demonstrated in simulated event samples that  $\hat{\omega}_{\min}$  and  $\chi_{\min}$  considerably outperform  $\Delta\varphi_{\min}^*$  and  $\Delta\varphi_i$  in rejecting QCD multijet background events and that  $\hat{\omega}_{\min}$  and  $\tilde{\omega}_{\min}$  can also be used to reduce the total standard model background events. In particular, large improvements were observed for a signal model with high jet multiplicity final states and with a compressed spectrum, in which events tend to have low to medium  $H_T$  and low  $H_T^{\text{miss}}$ .

We evaluated the performance only for one detector model, specified in the CMS detector configuration card in DELPHES. In order to quickly check the sensitivity of the performance to the detector model, we repeated the performance evaluation with the ATLAS detector configuration card, and we obtained nearly identical results, which is shown in Appendix B. However, as discussed in Appendix C, the jet  $p_T$  resolutions of the real CMS and ATLAS detectors might be better and have smaller tails than those of both DELPHES detector models, which potentially have a certain impact on the performance.





(a) Against the selection efficiency of the QCD background events



(b) Against the selection efficiency of the standard model (QCD + EWK) background events

**Figure 15:** The ROC curves showing the selection efficiencies of T1tttt(1950, 500) and T1tttt(1350, 1100) signal events against the selection efficiencies of (a) the QCD multijet background events and (b) the total standard model (QCD + EWK) background events for the conventional variables ( $\Delta\varphi_{\min 4}$ ,  $\Delta\varphi_{\min}^*$ ) and the alternative variables ( $\tilde{\omega}_{\min}$ ,  $\hat{\omega}_{\min}$ , and  $\chi_{\min}$ ) in three ranges of  $H_T$ . The markers indicate the values of the variables.

Furthermore, we evaluated the performance only for two signal models from a particular class of simplified SUSY models. These models have many jets in the final states. As the variables are designed to improve the signal acceptances of SUSY models with high jet multiplicity, we can naively expect that  $\hat{\omega}_{\min}$  and  $\chi_{\min}$  perform well for other signal models with high jet multiplicity. Nevertheless, it would be interesting to evaluate performances in a wide range of signal models.

We aimed to develop variables for QCD multijet background event suppression. However,  $\hat{\omega}_{\min}$  and  $\tilde{\omega}_{\min}$  turned out to be also useful in reducing the EWK background events, including  $Z(\rightarrow \nu\bar{\nu}) + \text{jets}$  events, which are usually considered irreducible. It might be possible to develop even better variables for EWK background event suppression if dedicated development is carried out.

In the event samples, 23 pileup interactions on average were included in each event. We have not studied the impact of varying the pileup interactions, which might influence the results.

We focused on all-hadronic final states in this paper. However, in searches in other final states, such as one lepton + jets + large  $E_{\text{T}}^{\text{miss}}$ , it is also important to reject events with large  $E_{\text{T}}^{\text{miss}}$  caused by a jet mismeasurement or neutrinos in hadron decays. In this case, as mentioned in Section 2, equivalent variables can be defined by replacing  $\vec{H}_{\text{T}}^{\text{miss}}$  with  $\vec{E}_{\text{T}}^{\text{miss}}$  in the definitions of  $\Delta\varphi_i$  and  $f_i$ . It is also possible to add  $\vec{p}_{\text{T}}$  of other objects, e.g., the lepton  $\vec{p}_{\text{T}}$ , to  $\vec{H}_{\text{T}}^{\text{miss}}$ .

The variables  $\tilde{\omega}_{\min}$ ,  $\hat{\omega}_{\min}$ , and  $\chi_{\min}$  are functions of  $\Delta\varphi_i$  and  $f_i$  of all jets in the event. In this paper, we considered only a specific form of the functions, i.e., these variables are each the minimum of some angles for all jets in the event whose tangents are the ratios of variations of  $H_{\text{T}}^{\text{miss}}$  and jet  $p_{\text{T}}$ , which can be written as functions of  $\Delta\varphi_i$  and  $f_i$ . It is probable that the best possible variable as a function of  $\Delta\varphi_i$  and  $f_i$  does not have this form. A variable with a somewhat different form is described in Appendix D. It might be possible to develop better dimensionless variables as a function of  $\Delta\varphi_i$  and  $f_i$ , for example, with machine learning algorithms.

Increasing the signal-to-background ratio is one of the most fundamental ways to improve the search for rare events. The alternative variables introduced in this paper can increase the signal-to-background ratio in SUSY searches. At the same time, it is important to continue to develop new variables so as to make the best use of the data at the LHC and future collider experiments.

## Acknowledgments

All simulated events used in this paper were produced in Data Intensive Computing Environment (DICE) at the University of Bristol Particle Physics Group. This work was supported by Science and Technology Facilities Council (UK).

**Note.** The code to calculate the alternative variables introduced in this paper can be found at <https://github.com/TaiSakuma/altdphi>.

## A Event selection with $\tilde{H}_{T\min}^{\text{miss}}$ and $X_{\min}$

It is suggested in Section 5 that  $\tilde{H}_{T\min}^{\text{miss}}$ , defined in Eq. (5.1), can possibly replace  $H_T^{\text{miss}}$  (or  $E_T^{\text{miss}}$ ) in the event selection. We pursue this possibility in this appendix. In addition to  $\tilde{H}_{T\min}^{\text{miss}}$ , we consider another variable with the dimension of the momentum:

$$X_{\min} \equiv H_T^{\text{miss}} \min_{i \in \text{jets}} (\tan \chi_i), \quad (\text{A.1})$$

where  $\chi_i$  is defined in Eq. (7.6).

Figure 16 compares the ROC curves for  $H_T^{\text{miss}}$ ,  $\tilde{H}_{T\min}^{\text{miss}}$ , and  $X_{\min}$ . The event samples are the same as the one described in Section 4 except the  $H_T^{\text{miss}}$  requirement ( $H_T^{\text{miss}} \geq 200$  GeV) is not applied. While  $\tilde{H}_{T\min}^{\text{miss}}$  outperforms  $H_T^{\text{miss}}$  only for the tight selection,  $X_{\min}$  considerably outperforms  $H_T^{\text{miss}}$  and  $\tilde{H}_{T\min}^{\text{miss}}$  for a wide range of the selection efficiency.

For example, in the bottom left panel of Fig. 16, the  $H_T^{\text{miss}}$  requirement ( $H_T^{\text{miss}} \geq 200$  GeV) reduces the signal events to 40%. The variable  $X_{\min}$  can keep them around 60% at the same QCD background efficiency—20% improvement. This panel is for the lowest  $H_T$  range for T1tttt(1350, 1100), the model with the compressed spectrum. Most events in this model reside in this  $H_T$  range. It is generally challenging to keep the signal acceptance of a compressed model large. The variable  $X_{\min}$  or similar variables with the dimension of the momentum can be useful alternatives to  $H_T^{\text{miss}}$  or  $E_T^{\text{miss}}$  for searches for signals of models with compressed spectra.

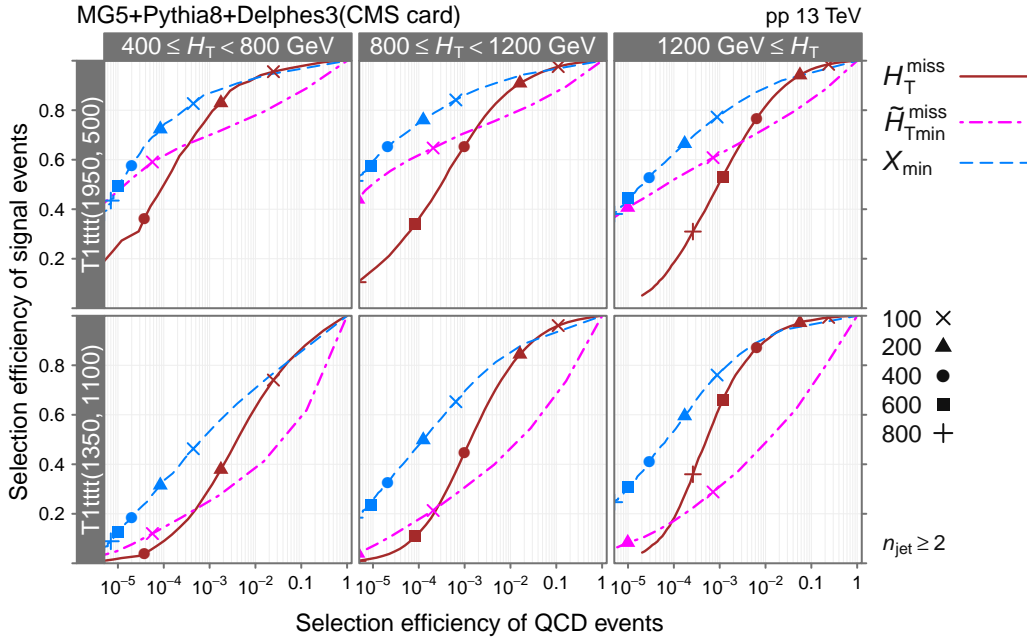


**Figure 16:** The ROC curves showing the selection efficiency of T1tttt(1950, 500) and T1tttt(1350, 1100) signal events against the QCD multijet background events for  $H_T^{\text{miss}}$ ,  $\tilde{H}_{T\min}^{\text{miss}}$ , and  $X_{\min}$  in three ranges of  $H_T$ . The markers indicate the values of the variables in GeV.

## B Performance in Delphes samples with ATLAS card

In the main body of this paper, we used the event samples simulated by DELPHES with the CMS detector configuration card as described in Section 4. We repeated the performance evaluation with the ATLAS detector configuration card. We used the configuration file `delphes_card_ATLAS_PileUp.tcl` included in the DELPHES package with a slight modification. The same number of the pileup interactions (23) were on average placed. The jet transverse momenta  $p_T$  were corrected in the same way.

We obtained nearly identical results. For example, Fig. 17 shows the ROC curves equivalent to Fig. 15a but with the ATLAS detector configuration card. The two figures look alike. We can draw the same conclusion as in Section 8.

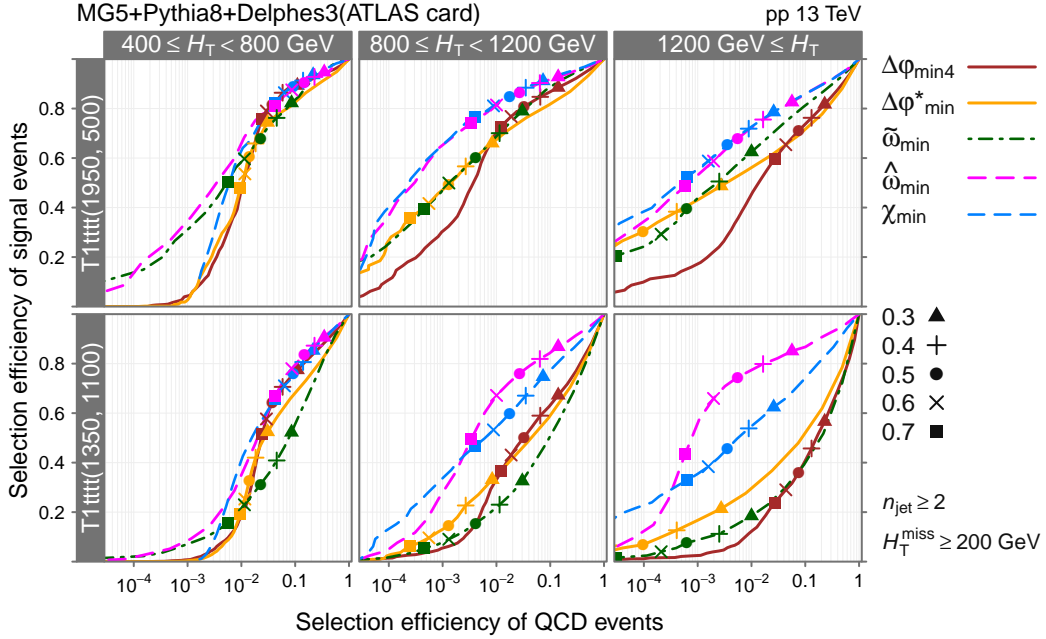


**Figure 17:** The ROC curves for the five variables against the selection efficiency of the QCD multijet background events, the equivalent of Fig. 15a but for the event samples simulated by DELPHES with the ATLAS detector configuration card.

However, in detail, all ROC curves in Fig. 17 are somewhat shifted towards right compared to those in Fig. 15a, indicating that the signal efficiencies with the ATLAS card are somewhat lower than with the CMS card at the same QCD background efficiency. This difference is in part due to the difference in the jet  $p_T$  resolutions between the two detector models, which will be discussed in Appendix C.

## C Jet $p_T$ resolution

Figure 18 compares the jet  $p_T$  resolutions of the two detector models, specified in the CMS and ATLAS configuration cards in DELPHES, in two ranges of the generated jet  $p_T$ . The

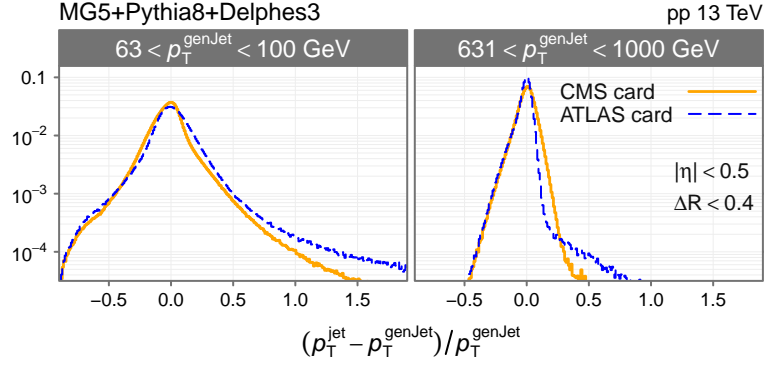


**Figure 18:** The jet  $p_T$  resolution: the distributions of  $((\text{jet } p_T) - (\text{generated jet } p_T))/(\text{generated jet } p_T)$  in QCD multijet events simulated by DELPHES with the CMS and ATLAS detector configuration cards in two ranges of generated jet  $p_T$ . A jet and generated jet within  $\Delta R = \sqrt{\Delta\varphi^2 + \Delta\eta^2} < 0.4$  are matched. Each distribution is normalized to unity.

peaks are at zero because that is how we corrected jet  $p_T$ . The distribution for the ATLAS configuration has a longer tail in the right side, which caused the minor difference in the ROC curves mentioned in Appendix B.

Somewhat equivalent figures in the CMS experiment can be found in Figure 35 of Ref. [39], in which the  $p_T$  ranges and the number of the pileup interactions are moderately different from what we used in Fig. 18. However, according to Figure 36 of the same reference, we can assume that the impact of these differences is not significantly large. The collision energy is also different. However, we can assume its impact is not significantly large either.

On these assumptions, it can be inferred that the jet  $p_T$  resolutions in the DELPHES samples used in this paper are worse than those in the CMS experiment. Furthermore, the shapes of the distributions and the sizes of the tails are also different. In fact, the difference between the distributions for the two detector configurations of DELPHES shown in Fig. 18 is smaller than the difference from the distributions in the CMS experiment shown in Figure 35 of Ref. [39]. These differences can potentially have a certain impact on the performance of the alternative variables introduced in this paper.

## D Alternative angular variable $\xi$

This appendix introduces yet another angular variable, which we let  $\xi$  denote. The ratio  $h_i$  is defined as

$$h_i = \begin{cases} g_i & \text{for } i \text{ that minimizes } \sin \Delta\tilde{\varphi}_i \\ f_i & \text{otherwise.} \end{cases}$$

The variable  $\xi$  is defined such that

$$\tan \xi \equiv \frac{\min_{i \in \text{jets}} \sin \Delta \tilde{\varphi}_i}{\max_{i \in \text{jets}} h_i}.$$

This ratio is the equivalent of  $1/f_{\text{max}}$  after  $H_{\text{T}}^{\text{miss}}$  is minimized by the variation of the jet  $p_{\text{T}}$  that minimizes  $H_{\text{T}}^{\text{miss}}$  most. In the DELPHES samples used in this paper, the variable  $\xi$  performs better than  $\Delta\varphi_{\text{min}}^*$  and  $\Delta\varphi_{\text{min}4}$ , but not better than  $\hat{\omega}_{\text{min}}$  or  $\chi_{\text{min}}$ .

## References

- [1] CMS collaboration, *Search for supersymmetry in multijet events with missing transverse momentum in proton-proton collisions at 13 TeV*, *Phys. Rev.* **D96** (2017) 032003, [[1704.07781](#)].
- [2] CMS collaboration, *Search for new phenomena with the MT2 variable in the all-hadronic final state produced in proton-proton collisions at  $\sqrt{s} = 13$  TeV*, *Eur. Phys. J.* **C77** (2017) 710, [[1705.04650](#)].
- [3] CMS collaboration, *Search for direct production of supersymmetric partners of the top quark in the all-jets final state in proton-proton collisions at  $\sqrt{s} = 13$  TeV*, *JHEP* **10** (2017) 005, [[1707.03316](#)].
- [4] CMS collaboration, *Search for the pair production of third-generation squarks with two-body decays to a bottom or charm quark and a neutralino in proton-proton collisions at  $\sqrt{s} = 13$  TeV*, *Phys. Lett.* **B778** (2018) 263–291, [[1707.07274](#)].
- [5] ATLAS collaboration, *Search for new phenomena with large jet multiplicities and missing transverse momentum using large-radius jets and flavour-tagging at ATLAS in 13 TeV pp collisions*, *JHEP* **12** (2017) 034, [[1708.02794](#)].
- [6] ATLAS collaboration, *Search for supersymmetry in events with b-tagged jets and missing transverse momentum in pp collisions at  $\sqrt{s} = 13$  TeV with the ATLAS detector*, *JHEP* **11** (2017) 195, [[1708.09266](#)].
- [7] ATLAS collaboration, *Search for a scalar partner of the top quark in the jets plus missing transverse momentum final state at  $\sqrt{s}=13$  TeV with the ATLAS detector*, *JHEP* **12** (2017) 085, [[1709.04183](#)].
- [8] CMS collaboration, *Search for Higgsino pair production in pp collisions at  $\sqrt{s} = 13$  TeV in final states with large missing transverse momentum and two Higgs bosons decaying via  $H \rightarrow b\bar{b}$* , *Phys. Rev.* **D97** (2018) 032007, [[1709.04896](#)].
- [9] CMS collaboration, *Search for supersymmetry in proton-proton collisions at 13 TeV using identified top quarks*, *Phys. Rev.* **D97** (2018) 012007, [[1710.11188](#)].
- [10] ATLAS collaboration, *Search for Supersymmetry in final states with missing transverse momentum and multiple b-jets in proton-proton collisions at  $\sqrt{s} = 13$  TeV with the ATLAS detector*, [[1711.01901](#)].
- [11] ATLAS collaboration, *Search for dark matter and other new phenomena in events with an energetic jet and large missing transverse momentum using the ATLAS detector*, *JHEP* **01** (2018) 126, [[1711.03301](#)].

- [12] ATLAS collaboration, *Search for squarks and gluinos in final states with jets and missing transverse momentum using  $36\text{ fb}^{-1}$  of  $\sqrt{s}=13\text{ TeV}$   $pp$  collision data with the ATLAS detector*, [1712.02332](#).
- [13] CMS collaboration, *Search for physics beyond the standard model in events with high-momentum Higgs bosons and missing transverse momentum in proton-proton collisions at  $13\text{ TeV}$* , [1712.08501](#).
- [14] CMS collaboration, *Search for natural and split supersymmetry in proton-proton collisions at  $\sqrt{s} = 13\text{ TeV}$  in final states with jets and missing transverse momentum*, [1802.02110](#).
- [15] CMS collaboration, *Search for Supersymmetry in  $pp$  Collisions at  $7\text{ TeV}$  in Events with Jets and Missing Transverse Energy*, *Phys. Lett. B* **698** (2011) 196–218, [[1101.1628](#)].
- [16] CMS collaboration, *Search for top squark pair production in compressed-mass-spectrum scenarios in proton-proton collisions at  $\sqrt{s} = 8\text{ TeV}$  using the  $\alpha_T$  variable*, *Phys. Lett. B* **767** (2017) 403–430, [[1605.08993](#)].
- [17] CMS collaboration, *A search for new phenomena in  $pp$  collisions at  $\sqrt{s} = 13\text{ TeV}$  in final states with missing transverse momentum and at least one jet using the  $\alpha_T$  variable*, *Eur. Phys. J. C* **77** (2017) 294, [[1611.00338](#)].
- [18] CMS collaboration, *Search strategy for exclusive multi-jet events from supersymmetry at CMS*, Tech. Rep. CMS-PAS-SUS-09-001, 2009.
- [19] CMS collaboration, *Performance of Methods for Data-Driven Background Estimation in SUSY Searches*, Tech. Rep. CMS-PAS-SUS-10-001, 2010.
- [20] L. Randall and D. Tucker-Smith, *Dijet Searches for Supersymmetry at the LHC*, *Phys. Rev. Lett.* **101** (2008) 221803, [[0806.1049](#)].
- [21] J. Alwall, R. Frederix, S. Frixione, V. Hirschi, F. Maltoni, O. Mattelaer et al., *The automated computation of tree-level and next-to-leading order differential cross sections, and their matching to parton shower simulations*, *JHEP* **07** (2014) 079, [[1405.0301](#)].
- [22] R. D. Ball et al., *Parton distributions with LHC data*, *Nucl. Phys. B* **867** (2013) 244–289, [[1207.1303](#)].
- [23] T. Sjöstrand, S. Ask, J. R. Christiansen, R. Corke, N. Desai, P. Ilten et al., *An Introduction to PYTHIA 8.2*, *Comput. Phys. Commun.* **191** (2015) 159–177, [[1410.3012](#)].
- [24] J. Alwall et al., *Comparative study of various algorithms for the merging of parton showers and matrix elements in hadronic collisions*, *Eur. Phys. J. C* **53** (2008) 473–500, [[0706.2569](#)].
- [25] P. Artoisenet, R. Frederix, O. Mattelaer and R. Rietkerk, *Automatic spin-entangled decays of heavy resonances in Monte Carlo simulations*, *JHEP* **03** (2013) 015, [[1212.3460](#)].
- [26] J. Alwall, P. Schuster and N. Toro, *Simplified Models for a First Characterization of New Physics at the LHC*, *Phys. Rev. D* **79** (2009) 075020, [[0810.3921](#)].
- [27] D. Alves, N. Arkani-Hamed, S. Arora, Y. Bai, M. Baumgart, J. Berger et al., *Simplified Models for LHC New Physics Searches*, *J. Phys. G* **39** (2012) 105005, [[1105.2838](#)].
- [28] CMS collaboration, *Interpretation of Searches for Supersymmetry with simplified Models*, *Phys. Rev. D* **88** (2013) 052017, [[1301.2175](#)].
- [29] ATLAS collaboration, *Search for top and bottom squarks from gluino pair production in final states with missing transverse energy and at least three  $b$ -jets with the ATLAS detector*, *Eur. Phys. J. C* **72** (2012) 2174, [[1207.4686](#)].



- [30] CMS collaboration, *Search for physics beyond the standard model in events with two leptons of same sign, missing transverse momentum, and jets in proton-proton collisions at  $\sqrt{s} = 13$  TeV*, *Eur. Phys. J.* **C77** (2017) 578, [[1704.07323](#)].
- [31] CMS collaboration, *Search for Supersymmetry in  $pp$  Collisions at  $\sqrt{s} = 13$  TeV in the Single-Lepton Final State Using the Sum of Masses of Large-Radius Jets*, *Phys. Rev. Lett.* **119** (2017) 151802, [[1705.04673](#)].
- [32] ATLAS collaboration, *Search for supersymmetry in final states with two same-sign or three leptons and jets using  $36\text{ fb}^{-1}$  of  $\sqrt{s} = 13$  TeV  $pp$  collision data with the ATLAS detector*, *JHEP* **09** (2017) 084, [[1706.03731](#)].
- [33] CMS collaboration, *Search for supersymmetry in events with one lepton and multiple jets exploiting the angular correlation between the lepton and the missing transverse momentum in proton-proton collisions at  $\sqrt{s} = 13$  TeV*, [1709.09814](#).
- [34] CMS collaboration, *Search for supersymmetry in events with at least three electrons or muons, jets, and missing transverse momentum in proton-proton collisions at  $\sqrt{s} = 13$  TeV*, *JHEP* **02** (2018) 067, [[1710.09154](#)].
- [35] DELPHES 3 collaboration, J. de Favereau, C. Delaere, P. Demin, A. Giammanco, V. Lemaître, A. Mertens et al., *DELPHES 3, A modular framework for fast simulation of a generic collider experiment*, *JHEP* **02** (2014) 057, [[1307.6346](#)].
- [36] M. Cacciari, G. P. Salam and G. Soyez, *The Anti- $k(t)$  jet clustering algorithm*, *JHEP* **04** (2008) 063, [[0802.1189](#)].
- [37] M. Cacciari, G. P. Salam and G. Soyez, *FastJet User Manual*, *Eur. Phys. J.* **C72** (2012) 1896, [[1111.6097](#)].
- [38] M. Cacciari and G. P. Salam, *Dispelling the  $N^3$  myth for the  $k_t$  jet-finder*, *Phys. Lett.* **B641** (2006) 57–61, [[hep-ph/0512210](#)].
- [39] CMS collaboration, *Jet energy scale and resolution in the CMS experiment in  $pp$  collisions at 8 TeV*, *JINST* **12** (2017) P02014, [[1607.03663](#)].